

Role of ammonia chemistry and coarse mode aerosols in global climatological inorganic aerosol distributions

Chao Luo¹, Charles S. Zender¹, Huisheng Bian², Swen Metzger³

Abstract

We use an inorganic aerosol thermodynamic equilibrium model in a three-dimensional chemical transport model to understand the roles of ammonia chemistry and natural aerosols on the global distribution of aerosols. The thermodynamic equilibrium model partitions gas-phase precursors among modeled aerosol species self-consistently with ambient relative humidity and natural and anthropogenic aerosol emissions during the 1990s.

Model simulations show that accounting for aerosol inorganic thermodynamic equilibrium, ammonia chemistry and dust and sea-salt aerosols improve agreement with observed SO_4 , NO_3 , and NH_4 aerosols especially at North American sites. This study shows that the presence of sea-salt, dust aerosol and ammonia chemistry significantly increases sulfate over polluted continental regions. In all regions and seasons, representation of ammonia chemistry is required to obtain reasonable agreement between modeled and observed sulfate and nitrate concentrations. Observed and modeled correlations of sulfate and nitrate with ammonium confirm that the sulfate and nitrate are strongly coupled with ammonium. SO_4 concentrations over East China peak in winter, while North American SO_4 peaks in summer. Seasonal variations of NO_3 and SO_4

¹ Department of Earth System Science, University of California, Irvine 92697, USA.

² Goddard Earth Sciences and Technology Center, University of Maryland-Baltimore county, NASA. Goddard Space Flight Center, Greenbelt, Maryland, USA.

³ Max-Planck-Institute for chemistry, Mainz, Germany.

are the same in East China. In North America the seasonal variation is much stronger for NO_3 than SO_4 and peaks in winter.

Natural sea salt and dust aerosol significantly alter the regional distributions of other aerosols in three main ways. First, they increase sulfate formation by 10-70% in polluted areas. Second, they increase modeled nitrate over oceans and reduce nitrate over Northern hemisphere continents. Third, they reduce ammonium formation over oceans and increase ammonium over Northern Hemisphere continents. Comparisons of SO_4 , NO_3 and NH_4 deposition between pre-industrial, present, and year 2100 scenarios show that the present NO_3 and NH_4 deposition are twice pre-industrial deposition and present SO_4 deposition is almost five times pre-industrial deposition.

1. Introduction

Tropospheric aerosols pose the largest uncertainties in estimates of climate forcing by anthropogenic changes to the atmosphere's composition [National Research Council (NRC), 1996]. Atmospheric aerosols are usually mixtures of many components, partly composed of inorganic acid (e.g. H_2SO_4 , HNO_3), their salts (e.g. $(NH_4)_2SO_4$, NH_4NO_3), and water [Charlson et al., 1978; Heintzenberg, 1989]. A couple of years ago, multicomponent aerosol concentrations are not routinely calculated within global atmospheric chemistry or climate models yet. The reason is that simulations of these aerosol particles, especially those including semi-volatile components, require complex and computationally expensive thermodynamic calculations [Metzger, 2000; Metzger et al., 2002a]. For instance, the aerosol-associated water depends on the composition of the

particles, which is determined by gas/liquid/solid partitioning, which is in turn strongly dependent on temperature and relative humidity [Metzger, 2000]. This study focuses on the roles of ammonia chemistry in multicomponent aerosol formation and partitioning, and on the sensitivity of this partitioning to the presence of coarse mode natural aerosols sea salt and mineral dust.

In the past two decades much effort has been devoted to the development of methods for the calculation of aerosol properties that are difficult to measure. These properties include the aerosol phase composition (i.e., solid or liquid) and the aerosol-associated water mass. Most studies have focused on the dominant inorganic aerosol compounds such as sulfate, ammonium, nitrate, and aerosol water [Metzger, et al., 2002b]. These compounds partition between the liquid-solid aerosol phase and gas phase aerosol precursor gases such as HNO_3 , and NH_3 . Numerous inorganic thermodynamic models have been developed to represent these processes. Some of them used the box model to estimate gas/aerosol partitioning [e.g., Kim et al., 1993a, 1993b; Kim and Seinfeld, 1995; Meng and Seinfeld, 1996; Nenes et al., 1998; Clegg et al., 1998a, 1998b; Jacobson et al., 1996; Jacobson, 1999; Meng et al., 1998; Sun and Wexler, 1998, Pilinis et al., 2000; Trebs, et al., 2005; Metzger et al., 2006], and some of them implemented simplify thermodynamic equilibrium model in global CTM model to simulate aerosol distributions [Metzger et al, 2002a, 2002b; Rodriguez and Dabdub, 2004; EMEP 2003; Lauer et al., 2005; Tsigaridis, et al., 2006]. The differences between our model and these models are the meteorological data, resolution, emission, transport, deposition, chemistry, and ect.. For example, Metzger et al. [2002b] used European Center for Medium-range

Weather Forecasts (ECMWF), resolution is 2.5x2.5; and Rodriguez et al. [2004] used monthly mean meteorological data with resolution 5x5. The numerical advection in our model is calculated by second-order moments method [Pater, 1986]. As we show below, these processes, such as meteorology, chemistry, and etc., are important for self-consistent treatment of biogeochemical air-surface exchanges, e.g., N deposition.

This paper is organized into four sections. Section 2 briefly describes the models used in this study. Section 3 compares our climatological predictions to observations and presents our sensitivity studies. Section 4 summarizes the study.

2. Model description

2.1 Global chemistry transport model

This study use the UC Irvine global chemistry transport model (UCICTM) [Prather et al., 1987; Jacob et al., 1997; Olsen et al., 2000; and Bian and Prather 2003; Bian and Zender 2003] with an embedded aerosol equilibrium model [Metzger et al., 2002a]. The UCICTM includes an O₃-NO_x-NMHC-SO₂ chemical scheme with 48 species, 95 chemical kinetic reactions, 22 photolytic reactions, and 9 aqueous reactions upgraded with ammonia chemistry, dust and sea salt modules. [Wild and Prather, 2000; Wild and Akimoto, 2001; Bian 2001]. Trace gas emissions are based on the aeroCOM emissions Inventory Activity database [<http://www.mnp.nl/edgar/model/edgarv32/acidifying>]. A first-order rainout parameterization for soluble gases and particles is used for large-scale precipitation [Giorgi and Chameides, 1986]. Scavenging of aerosol by convective precipitation is computed in the model as part of the convective mass transport operator [Bian, 2001]; air pumped in wet convective updrafts loses a fraction of its aerosol to

deposition before dispersing at the top of the updraft. We adopt here a 50% aerosol scavenging efficiency in shallow wet convection (extending up to ~2600 m altitude) and a 100% scavenging efficiency in deep wet convection [Balkanski et al., 1993]. Dry deposition of gases and aerosols is calculated with a resistance-in-series scheme [Wesely and Hicks, 1977], and gravity settling deposition for large dust and sea salt particles. The numerical solution for advection and convection conserved the second-order moments of tracer distribution (i.e., quadratics plus cross terms). The meteorological fields used in this study are from the Goddard Institute for Space Study (GISS) general circulation model version II that is run with a resolution of 4 degree latitude by 5 degree longitude, and 9 vertical levels. These meteorological fields include 3-D (winds, temperature, water vapor, clouds, and convection) and 2-D (boundary layer properties) data at 3-hours averages. The scope of this study is focused on the impacts of chemical transformation on gas-aerosol partitioning and distribution with a single climatological meteorological field. We did not explore the impacts of different meteorological fields and model resolution on simulations. The impacts of different meteorological fields and different resolutions were explored using same model by GISS GCM 9 levels (GISS9) and GISS GCM 23 levels (GISS23) and European Center for Medium-range Weather Forecasts (EC21) [Bian, 2001]. In her experiments, the vertical resolution did impact Rn and Pb concentration especially over land source regions. Overall using the meteorological fields with two different vertical resolutions gave similar conclusions for Rn's spatial and temporal distributions. [Bian, 2001]. The relative biases of simulated Rn column by GISS9 meteorological field are around 7%-15% globally [Bian, 2001]. Even Rn simulations by

GISS9 meteorological field doesn't do well seasonal cycle over most land stations as simulated by GISS23 and EC21 meteorological fields, but the seasonal cycle simulated by GISS9 meteorological field are still reasonable at most sites [Bian, pp 138, pp160, pp 171-176, PhD thesis, 2001].

Aerosols are included here in the calculation of photolysis rate using the multiple-scattering Fast-J scheme [Wild et al., 2000; Bian and Prather, 2002], which explicitly accounts for aerosol and cloud optical properties. In each CTM layer the monthly mean aerosol extinction is combined with the 3-hour cloud optical depths from the meteorological fields. Fast-J is computationally efficient, and the radiation field as a function of wavelength is calculated hourly throughout the entire column. Bian and Zender [2003] document the seasonal and regional roles of aerosol-influenced photolysis on important atmospheric oxidants. Instead of a prescribe tropopause (used to diagnose where tropospheric versus stratospheric chemistry was calculated) and an upper boundary flux O₃, the CTM model dynamically diagnoses the tropopause by using an on-line, ozone-like tracer (Syn-O₃) with an effective source of 475 Tg/yr in the highest level of the model and was removed at surface [McLinden et al., 2000; Hannegan, 2000]. The model has been applied previously to simulations of both tropospheric and stratospheric chemistry and transport [Prather et al., 1987; Hall and Prather, 1993; Avallone and Prather, 1997; Jacob et al., 1997; Hannegan et al., 1998; Hsu et al., 2004; Olsen et al., 2000; McLinden et al., 2000, 2003; Bian et al., 2001, 2003; Wild et al., 2000, 2003, 2004]. The tropospheric model has been evaluated in several publications: tropospheric O₃ and CO, NO_x/NO_y at Mauna Loa, and global peroxyacetylnitrate (PAN) profiles of

Wild and Prather [2000], and Wild and Akimoto [2001], further O₃ and CO evaluations of IPCC 2001 [Prather and Ehhalt, 2001], and updated radon and lead simulations of Bian [2001].

2.2 Emissions

We map the AEROCOM emission inventories (SO_x, NO_x) to the model grid, preserving the second-order moments of the emissions. Additional emissions for CO and biomass burning sources are from Wang et al. [1998a]. NO from lightning is based on the parameterization of Price and Rind [1992]. A NO source from aircraft is also included [Baughcum et al., 1996]. The ammonia cycle was calculated by adding gas phase ammonia (NH_3) and aerosol ammonium (NH_4). Recent GEIA ammonia emissions inventory was used in the model [Bouwman et al., 1997]. The total ammonia source was estimated to be 53.6 Tg N/yr. And most of them are from domesticated animals (43.3%), and fertilizers (16.8%).

2.3 Mineral dust

The mineral aerosols sources are calculated using Dust Entrainment And Deposition [Zender et al., 2003]. This mobilization scheme is based on the wind tunnel and in situ studies of Iversen and White [1982], Marticorena and Bergametti [1995], Gillette et al., 1998], and Fecan et al., 1999]. It is similar to those used in Tegen and Fung [1994], Mahowald et al., [1999], Ginoux et al., [2001], and Tegen et al., [2002] in that it is based on a wind threshold velocity and has a wind speed cubed relationship for dust mobilization, but the detail of the mobilization are slightly different in each case. Four size bins of dust from 0.1-10 um are independently predicted. Within each bin we assume

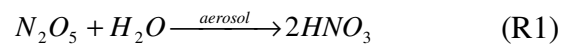
log-normal distribution in aerosol sizes [Zender et al., 2003].

2.4 Sea Salt

The dominant mechanism for sea-salt production over the open ocean is believed to be air bubbles bursting during whitecap formations [Blancnchard and Woodcock, 1980]. Sea spray is generated by the wind stress on the ocean surface. Air bubbles, which constitute the whitecaps resulting from breaking waves, burst at the water surface and produce small droplets by means of two mechanisms. Film drops are produced when the thin liquid film that separates the air within a bubble from the atmosphere ruptures. The remaining surface energy of the bubble, after bursting, results in a liquid jet that becomes unstable and breaks into a number of jet drops (Smith et al., 1993). The formation of film and jet drops is called the indirect mechanism. At wind speeds greater than 10–12 m s⁻¹, spume drops torn directly from the wave crests by the strong turbulence make an increasing contribution to the sea salt and dominate the concentration at larger particle sizes. The formation of spume drops is called the direct mechanism. We prescribe production of sea salt particles based on the Monahan et al. [1986] and Smith et al. [1993] empirical parameterization of laboratory experiments for both mechanisms.

2.5 Heterogeneous reactions module

Observations continue to highlight the importance of heterogeneous reactions on aerosol surface. The reactions of N_2O_5 and/or NO_3 on wet aerosol surfaces are likely to be responsible for the observed destruction reactions:



Based on the observations and models, we include SO_2 uptake on dust aerosol surface and form into sulfate, and NO_3 and N_2O_5 uptake on dust surface and form into nitrate [Zhang and Carmichael, 1999], and N_2O_5 uptake on aerosols (sulfate, nitrate, ammonium, and sea salt) form to HNO_3 [Dentener and Crutzen, 1993; Dentener et al., 1996; and Bian and Zender, 2003]. The heterogeneous reactions and uptake coefficients used in our model are same as Bian and Zender [2003]. Uncertainties in uptake coefficients are large, up to three orders of magnitude for certain species [Michel et al., 2002]; Underwood et al. 2001; and Zhang and Carmichael 1999; Bian and Zender 2003]. For example, recent studies report $2.0 \times 10^{-5} < \gamma < 1.6 \times 10^{-2}$ for HNO_3 [Goodman et al., 2000; Underwood et al., 2001]. We apply the values in globally so that regional differences in uptake coefficients due to dust mineralogy and RH are neglected. Our results on heterogeneous uptake on aerosol for some species should be considered an upper bound since some of these species would be lost to heterogeneous reactions on other aerosol types.

Our model includes the optical effects of BC/OC species on photolysis but neglects heterogeneous chemistry on BC/OC. Heterogeneous chemistry of carbonaceous particles is complex [Seinfeld J., S. Pandis, P708, 1997] and currently beyond the UCICM capabilities. Since the uptake coefficients are highly uncertain, it is difficult to assess the impact of neglecting these reactions. But impacts of ignoring heterogeneous reactions on BC/OC could be important in high BC/OC emission areas, such as East Asia, South Africa and South America.

2.6 Aerosol equilibrium thermodynamics module

This study uses the Equilibrium Simplified Aerosol model (EQSAM) model [Metzger, 2000; Metzger et al., 2002a, 2002b, Metzger et al., 2006]. The module includes the ammonium-sulfate-nitrate-water and major crustal elements (Ca^{2+} , Mg^{2+} , K^+) and sea salt (Na^+ , and Cl^-). EQSAM assumes that aerosols are internally mixed and obey thermodynamic gas/aerosol equilibrium. These assumptions are accurate under most atmospheric conditions considering the one hour time steps used in UCICTM. The basic concept of EQSM is that the activities of atmospheric aerosols in equilibrium with the ambient air are governed by relative humidity (RH). Since the water activity is fixed by RH, the solute activity is, for a given aerosol composition, a function of RH; the molality depends on the water mass, which solely depends on RH. This is also approximately true for activity coefficients of salt solutes of binary and multicomponents solutions. Using the “domain structure” [Sven Metzger et al., 2002a], and taking into account that gas/aerosol equilibrium is only valid for certain domains where sulfate is completely neutralized, we can noniteratively calculate the aerosol composition, including aerosol-associated water. The equilibrium assumption further implies that the water activity (a_w) of an aqueous aerosol particle is equal to the ambient relative humidity (RH), i.e., $a_w = RH$ [Bassett and Seinfeld, 1983] which the UCICTM supplies. This is valid for atmospheric applications, since the ambient relative humidity is not influenced by the small water uptake of aerosol particles. Because sulfuric acid has a very low vapor pressure, it is assumed that it resides completely in the aerosol phase.

Certain salts, such as ammonium sulfate or ammonium nitrate, deliquesce if the relative humidity reaches a threshold value; below the value these salts may be

crystalline. Deliquescence of various salt compounds is determined in EQSAM in the corresponding subdomains [Metzger, 2000; Metzger et al., 2002a]. The deliquescence of salt aerosol depends on the ambient RH and temperature. For partitioning between the gas/liquid/solid aerosol phases, chemical equilibrium is determined by the temperature dependent equilibrium constant.

2.7 Measurements

Comparisons of simulated total aerosol mass concentrations for sulfate, nitrate and ammonium with measurements from two different available databases are presented in this section. Aerosol observations made from 1987 to 1999 at more than 70 monitoring stations across North America are available from CASTNET website (<http://www.epa.gov/castnet/data.html>). In addition, a comparable dataset that corresponds to European measurements was obtained from EMEP (<http://www.nilu.no/projects/ccc/emepdata.html>) [Hjellbrekke, 2000]. EMEP reported measurements are obtained from annual averages that span from 1978 to 2000. The measurements at Bermuda, Oahu, Okinawa, and Cheju (University of Miami observation network) are used for the model evaluation. Model results represent atmospheric concentrations of species during a typical year of the 1990 decade. Therefore arithmetic means from CASTNET and EMEP datasets and data from University of Miami observation network are used for comparison with model outputs instead of data from any specific year.

3. Model results

3.1 Global aerosol distribution

The following section analyzes the predictions of the UCICTM coupled with EQSAM. In addition, evaluation of the coupled model against available data at ground-based stations in North America and Europe is provided to assess model performance. Annually averaged concentrations at the surface level for major species simulated with the coupled UCICTM-EQSAM are shown in Figure 1. The aerosol distributions are similar to the distribution of the aerosol precursors. High SO_2 and HNO_3 are over industrialized areas, such as East Asia, Europe, and North America. In general, the model reproduces well known features of secondary aerosol distributions such as high sulfate, nitrate and ammonium over industrialized regions [Benkovitz et al., 1994; Chin et al., 1996; Rodriguez and Dabdub 2004; Metzger, et al., 2002b]. For instance, annual average concentrations of sulfate, nitrate, and ammonium are high over industrialized regions, such as the east coast of China, central Asia, Europe and North America, consistent with high emissions in these regions. Their values could reach 6-15 $\mu g m^{-3}$ for sulfate, 4-9 $\mu g m^{-3}$ for nitrate, and 4-6 $\mu g m^{-3}$ for ammonium. Dust concentrations are distributed over North Africa, Arabian peninsular, East Asia, and Australia, which is similar with the previously calculations [Zender et al., 2003; Luo et al., 2003; Mahowald et al., 2003; Ginoux et al., 2001] (figure 1) . Model underpredicts dust concentration over East Asia. Sea salt concentrations are high over the middle latitude of Southern and Northern Oceans and Arctic regions (figure 1).

It is important to consider the fidelity of the model performance against direct station measurements of aerosol concentration. The root-mean square (RMS) absolute error

RMS_{abs} is computed as

$$RMS_{abs} = \sqrt{\frac{1}{N} \sum_{i=1}^N (x_i - y_i)^2} \quad (E1)$$

where x_i are observed data and y_i are modeled data. The RMS_{abs} is a strict measure of absolute model bias against the observed aerosol concentration. The stations with greatest absolute concentrations dominate RMS_{abs} when it is computed using untransformed (linear) data. We also computed RMS_{abs} with logarithmically transformed data, i.e., using $\log x$ and $\log y$ in place of x and y in equation E1, and we compared the two error estimates. The differences were small, so we only include RMS_{abs} using untransformed (linear) data in Table 3. The final statistic we examined is the relative root-mean square bias, RMS_{rel} . RMS_{rel} is computed from the relative, rather than absolute, bias for each experiment

$$RMS_{rel} = \sqrt{\frac{1}{N} \sum_{i=1}^N \left(\frac{x_i - y_i}{x_i}\right)^2} \quad (E2)$$

The relative root-mean square biases are included in Table 3. The mean relative bias (MRB) is calculated

$$MRB = \frac{1}{N} \sum_{i=1}^N \left(\frac{x_i - y_i}{x_i}\right) \quad (E3)$$

and are included in Table 3 in order to show model simulation is in error for each experiment.

CASTNET and EMEP measurements of SO_2 , HNO_3 , and NH_3 (CASTNET does not measure NH_3) generally agree well with UCICM predictions (Figure 2).

Linear correlation coefficients between observations and simulations of SO_2 and

HNO_3 are over 0.69 and 0.67 in North America and 0.46, 0.54 in Europe respectively. The correlation coefficients between observations and control simulations (CTL) are 0.81, 0.41, and 0.74 for sulfate, nitrate and ammonium respectively in north America and 0.45, 0.67, and 0.46 respectively in Europe (Figure 3, and Table 2). Both our UCICTM climatological results and previous study from a completely different CTM (IMAGE) and aerosol equilibrium model (SCAPE2) [Rodriguez and Donald 2004], show that comparisons are better at CASTNET than at EMEP.

The discrepancy between the UCICTM and observations is larger over the European EMEP sites than the north American CASTNET sites (Figure 3, also see figure5a, 5b,5c and Table 2, and Table 3), similar to the bias in Rodriguez and Dabdub [2004]. Similar as our results, Rodriguez's comparisons show that data dispersion is larger over sites of EMEP (Europe) [Rodriguez, and Dabdub, 2004]. It could suggest that this discrepancy couldn't be caused by meteorological data, since we used different meteorological datasets. This could be due to emission biases or model deficiencies, e.g. due to missing aerosol compounds in EQSAM. The uncertainties of the combined sampling and chemical analysis of EMEP measurements are range from 15-20% (<http://www.nilu.no/projects/ccc/ga/index.htm>). The uncertainties of CASTNET measurements are around 5% for sulfate and 10-12% for nitrate and ammonium (<http://cfpub.epa.gov/gdm/index.cfm>). That could be one of reasons why model comparisons are better at CASTNET sites than at EMEP sites. To further evaluate model performance, we compare the correlations of species of sulfate, nitrate, and ammonia of observations and simulations to show the degree to which these chemical cycles are

coupled (Figure 4 and Table 1).

Sulfate and ammonium are very tightly correlated in both observations ($r > 0.8$) and in the UCICTM ($r > 0.9$). The observed correlation coefficient of SO_4 and NH_4 is over 0.9 at CASTNET (North American) sites, and falls to 0.81 including all CASTNET and EMEP sites. It suggests that variability of $(NH_4)_2SO_4$ or/and NH_4HSO_4 explain 80% of the variability of sulfate. There is high correlation between nitrate and ammonium (0.71 for observation and 0.57 for model simulation). This suggests roughly half of the variability of nitrate can be explained by NH_4NO_3 variability. The small observed and modeled correlations between sulfate and nitrate ($r=0.52$ and 0.49 , respectively) reflect the fact that sulfate and nitrate precursor sources are distinct in space and time. Although the correlations are high for observations and model simulations, but the slopes are different. One reason could be that all observation data were collected in continents, but model data include continent and ocean. The partitioning could be different between continent and ocean, since anion and cation abundance are quite different over continent and over ocean. In figure 4, we highlight corresponding grids where observations are available for model simulations.

3.2 Seasonal variation

Globally the largest sulfate concentration is persistently presented over East China year around. Observed SO_4 concentrations didn't show stronger seasonal variation over European. Sulfate shows East China peak in winter (not shown here), while North American SO_4 peaks in summer (Figure 5a). China uses more coal for heating in winter

which results in maximal winter SO_4 . We calculate continental mean seasonal cycle of sulfate that show the mean stations and model prediction for Europe and North America (Left and right top panels in figure 5a). Continental mean seasonal cycles also show that sulfate didn't show strong seasonal variation in Europe and sulfate shows peak in summer in North America. Seasonal variations of NO_3 and SO_4 are the same in East China. In North America the seasonal variation is much stronger for NO_3 than SO_4 and peaks in winter. This is due to the greater reliance in North America on gas and oil for winter heating.

The ammonium seasonal variation is similar to the sulfate seasonal variation, highest in winter and smallest in fall for East China and Europe. The similar seasonal variations of ammonium and sulfate are consistent with the strong correlation between sulfate and ammonium noted previously.

Monthly variations between observations and model simulations at some sites of CASTNET and EMEP and sites of University of Miami observation network are shown in Figures 5a, 5b, and 5c. From figure 5a, 5b and 5c, it can be seen that the model capture the seasonal cycle at some sites, but not all sites. Comparison of Rn simulated with different meteorological fields (ECMWF, GISS21, and GISS9) shows that the GISS9 meteorology used here is most biased in the seasonal cycle over land stations [Bian, pp 171-176, PhD thesis, 2001]. The lack of winter sulfate over North America could be due to a large reduction of sulfuric acid production. In East Asia and especially China, sulfate may be higher in winter due to fossil fuel burning.

Regional variations in seasonal emission patterns have significant impacts on

aerosol production and partitioning. Low nitrate in summer could be caused by nitric acid and nitrate are more effectively removed in summer than in winter. Ammonium concentrations are higher in winter at some sites and higher in summer at other sites, depending on NH_3 , HNO_3 , H_2SO_4 and meteorological parameters. The model calculated higher sulfate and ammonium in January at EMEP sites (figure 5a, 5c) could be caused by uncertainties in meteorological data, since dynamic fields tend to have similar impacts on different species (sulfate and ammonium). Again the model biases are smaller at CASTNET (North America) sites than at EMEP (Europe) sites (figure 5a, 5b, 5c). As discussed above, these discrepancies between sites in America and Europe may not be caused by meteorological data and transport. Biases can also be due to emissions, deposition, or chemical mechanisms.

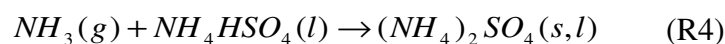
3.3 Sensitivity analysis

We now show the results of three sensitivity experiments to assess important aerosol formation processes. The standard (CTL) model described above includes the thermodynamic aerosol equilibrium model and ammonia chemistry interacting with coarse model natural aerosols (dust and sea salt). The first sensitivity experiment (XPT1) turns off thermodynamic equilibrium model. The second sensitivity experiment (XPT2) turns off ammonia chemistry (XPT2), and the third sensitivity experiment (XPT3) omits dust and sea salt aerosol.

Annual mean correlation coefficients of SO_4 , NO_3 , and NH_4 between observations and model simulations at EMEP and CASTNET sites worsen when inorganic aerosol thermodynamic partitioning is not applied especially for EMEP

measurements (compare Figure 3 and Figure 6, Table 2). The EQSAM aerosol module improves correlations between SO_4 simulations and observations at both EMEP and CASTNET sites (Figure 6, summarized in Table 2). EQSAM improves nitrate and ammonium simulations at CASTNET sites. However, accounting for inorganic aerosol partitioning produces little difference between CTL and XPT1 nitrate and ammonium simulations at EMEP sites (compare Figure 6 to Figure 3, summarized in Table 2) and it is unclear for the reason of this performance. The RMS and relative biases are strict measures of absolute model bias against the observed aerosol concentration. The regress parameters and model mean relative biases and RMS_{abs} and RMS_{rel} are summary in Table 2 and Table 3. From table 3, we can see that the root-mean square bias and mean relative bias of CTL are smaller than XPT1 experiment.

Ammonia chemistry (CTL) greatly improves SO_4 and NO_3 simulations at all sites (compare Figure 7 to Figure 3, summarized in Table 2, and Table 3). Ammonium sulfate and ammonium nitrate can be produced by follow reactions.



Experiments also show that H_2SO_4/H_2O system dose not nucleate easily but $NH_3/H_2SO_4/H_2O$ system does [Coffman and Hegg, 1995]. Our results demonstrate that ammonia chemistry is clearly very important for aerosol formation and partitioning (compare figure 3 with figure 7, table 2). This is consistent with Figure 4 which shows

correlations of sulfate and nitrate with ammonium range from 0.71-0.81 (observed) and 0.57-0.93 (simulated). Table 3 also shows bias of CTL is much smaller than bias of XPT2, which is the largest in CTL and all experiments runs. The positive mean relative biases for XPT2 in Table 3 reflect that the model calculated sulfate and nitrate are much smaller than observations, which is consistent with figure 7.

Coarse mode aerosols such as dust and sea salt provide ample surface area and liquid volume for significant heterogeneous chemistry (e.g., Dentener et al. 1996, Bian and Zender 2003), also are the sources of crustal elements such as Ca^{2+} , Mg^{2+} , K^+ , Na^+ , and Cl^- , which are important for aerosol partitioning [Kim et al., 1993a, 1993b; Kim and Seinfeld, 1995; Meng and Seinfeld, 1996; Nenes et al., 1998]. Hence removing dust and sea salt (XPT3) test the effect of these coarse aerosols on sulfate, nitrate and ammonium aerosol formation. Figure 8 shows that scatter plots of observation and XPT3 experiment. It can be seen that the correlations of XPT3 are almost similar to CTL simulation at EMEP sites, and worse than CTL simulation at CASTNET sites. Since sulfate proportional to dust and SO_2 is because SO_2 uptake on dust aerosol surface and form to sulfate by heterogeneous reactions included in our model. But other species such as NO_3 , and N_2O_5 are not behavior same way as SO_2 in the heterogeneous reactions. For example, nitrate can be produced by NO_3 heterogeneous reactions on the aerosol surface, but NO_3 and N_2O_5 are not necessarily removed as nitrate, but can also be lost from the aerosol as HNO_3 , and this decreases nitrate production. That may be the reason why the correlations of other species are same or better in XPT3 experiment. The

presence of dust and sea salt (CTL) significantly increases sulfate production and concentration by 10-70% in polluted continental regions such as East Asia, Europe, and part of America (see panel 1 of Figure 9). This is because SO_2 uptake on dust aerosol surface to form sulfate via heterogeneous reactions (Bian and Zender, 2003). The sulfate formation by heterogeneous reactions is proportional to dust and SO_2 concentrations and so sulfate concentration are higher in industrial areas, such as East Asia, Europe and North America. Sulfate increases less from 0-60S than in the northern hemisphere, consistent with inter-hemispheric SO_2 gradient. From figure 5a, we can see that the sulfate decrease almost at every sites without dust and sea salt (XPT3).

Nitrate formation decreases in polluted industrial regions, and increases over most ocean regions when dust and sea salt are present (Panel 2 of Figure 9). More HNO_3 loss on the surface of dust and sea salt aerosols in high pollution areas, and nitrate decreases in these areas could be due to less available HNO_3 to form nitrate, according to R1 and R2. Over ocean regions, N_2O_5 uptake may dominate nitrate formation.

Dust and sea salt increase ammonium concentration in polluted regions and decreases ammonium over most ocean regions and in the southern Hemisphere (Figure 9, panel 3). This reduction over ocean is partly explained by the presence of cation (N_aCl , M_gCl_2 , C_aCO_3) tied to sea salt and dust. The cation abundance makes it difficult for NH_3 to partition into the aerosol phase. In polluted regions, anion abundance (such as SO_4 , NO_3) allows NH_3 to easily partition into the aerosol phase.

Generally from previous validations, our simulations show model did the reasonable works, model captures seasonal cycles at some sites but not all sites, same as Rn simulations using same model and meteorological data [Bian, 2001]. The biases calculated by model simulations and observation at EMEP and CASTNET are shown in Table 3. It can be seen that biases of sulfate and nitrate are the smallest for control run, and then XPT1, XPT3, and XPT2. The biases of ammonium are the smallest for XPT3 experiment. As mentioned earlier, our model includes optical effects of BC/OC species on photolysis and neglects BC/OC heterogeneous chemistry. We expect any biases due to neglecting BC/OC heterogeneous chemistry to be largest in and near BC/OC emissions areas.

3.4 Deposition comparison

Deposition fluxes of SO_4 , NO_3 , and NH_4 aerosols are important for biogeochemistry cycles. Figure 10 shows the distributions of total predicted sulfate, nitrate and ammonium deposition (dry plus wet). High deposition rates occur in and downwind of industrial areas such as East Asia, Europe and North America. We compare depositions of sulfate, nitrate and ammonium against CASTNET-inferred deposition, which CASTNET calculates using observed concentrations and deposition velocity (Figure 11). It shows that model underpredicts depositions of sulfate, nitrate and ammonium, and are consistent of aerosol concentrations comparisons.

Table 4 compares SO_4 , NO_3 , NH_4 , NH_3 and HNO_3 of our simulations with previous studies, and it shows us our results are comparable with previous works. Deposition of ammonia is comparable with ammonium deposition. Ammonia wet deposition is at same magnitude as ammonium, but ammonia dry deposition can be 3-4

times of ammonium deposition. That is why the ammonium deposition is about half of total ammonia emission. Additionally we compare SO_4 , NO_3 , NH_4 , NH_3 and HNO_3 deposition between present and pre-industrial, and year 2100 scenarios. For the pre-industrial simulation, we turn off all anthropogenic emissions. Year 2100 emissions follow the B1 and A1B Intergovernmental Panel on Climate Change (IPCC) scenarios (IPCC Special Report on Emissions Scenarios, <http://www.grida.no/climate/ipcc/emission>). The meteorological fields are present-day, i.e., the same as the control (CTL), in both pre-industrial and Year 2100 simulations. We find that the present deposition of NH_4 and NO_3 are twice pre-industrial deposition and present SO_4 deposition is almost five times pre-industrial deposition.

4. Conclusions

We use a thermodynamic aerosol model in a three-dimensional chemical transport model to assess the roles of ammonia chemistry and coarse mode natural aerosol in the global distribution of sulfate, nitrate, and ammonia. Our model simulations generally reproduce observed aerosol concentrations and seasonal variations especially at North American and East Asia sites. The annually averaged sulfate falls within a factor of two of the observations at about 95% of CASTNET sites. The discrepancy between model and observation is larger for European sites. This discrepancy may be independent of meteorological fields, since simulations by Rodriguez and Dabdub [2004] led to similar results with different meteorological datasets. Sensitivity experiments show that accounting for aerosol inorganic thermodynamic equilibrium improves agreement with

observed SO_4 , NO_3 , and NH_4 aerosols especially at North American sites. The model bias of control run is the smallest for sulfate and nitrate among all experiments.

Moreover, with ammonia chemistry, dust and sea salt significantly increases sulfate production and concentrations in polluted regions. In all regions and seasons, representation of ammonia chemistry is required to obtain reasonable agreement between modeled and observed sulfate and nitrate concentrations. Observed and modeled correlations of sulfate and nitrate with ammonium confirm that the sulfate and nitrate are strongly coupled with ammonium.

Dust and sea salt increase nitrate concentrations over ocean regions where N_2O_5 uptake leads to increased nitrate formation. Dust and sea salt reduce nitrate concentrations over industrial and very dusty regions (e.g., North Africa) since HNO_3 is lost on dust surface, and less HNO_3 is available to form nitrate in polluted regions. Dust and sea salt increase ammonium formation in industrial regions and in very dusty regions, and they reduce ammonium over remote oceans. This reduction over ocean is partly explained by the presence of cation ($NaCl$, $MgCl_2$, $CaCO_3$) tied to sea salt and dust. The cation abundance makes it difficult for NH_3 to partition into the aerosol phase. In polluted regions, anion abundance (such as SO_4 , NO_3) allows NH_3 to easily partition into the aerosol phase. Our model neglects heterogeneous chemistry on BC/OC heterogeneous chemistry. We expect the largest biases due to neglecting heterogeneous reactions on BC/OC occur in high BC/OC emission areas, such as East Asia, South Africa, and South America.

Consistent with previous studies, we find high deposition rates of sulfate, nitrate, and ammonium occur in and downwind of industrial areas such as East Asia, Europe and North America. Additionally, we find that present deposition of NH_4 and NO_3 are twice pre-industrial deposition, and that present SO_4 deposition is almost five times pre-industrial deposition. We are currently using these atmospheric forcings to quantify anthropogenic impacts on the oceanic nitrogen and sulfur cycles.

Figure Caption:

Figure 1, Annual mean SO_2 , HNO_3 , NH_3 , sulfate, nitrate, and ammonium, dust and sea salt concentrations on surface level.

Figure 2, Model-observation comparisons of SO_2 , HNO_3 , NH_3 , in Europe and North America. Linear correlation coefficient r , and best fit parameters to $y=mx+b$, where x are observed data and y are simulated.

Figure 3, Model-observation comparisons of sulfate, nitrate and ammonium in Europe and north America for CTL simulation, statistics parameters are same as in figure 2.

Figure 4, Correlations of ammonium verse sulfate, ammonium verse nitrate, and nitrate verse sulfate for observation and model simulation, highlight corresponding grids where observations are available in the right column.

Figure 5a, Seasonal comparisons of sulfate concentration at some observed sites, black line represents control run, red line for XPT1, blue line for XPT2, and green line for XPT3 .

Figure 5b, Same as figure 5a, but for nitrate comparison.

Figure 5c, Same as figure 5a, but for ammonium.

Figure 6, Sulfate, nitrate and ammonium comparisons with EMEP and CASTNET observations for experiment XPT1 (without thermodynamic equilibrium module).

Compare to Figure 3, statistics parameters are same as figure 2, but for XPT1.

Figure 7, Sulfate and nitrate comparisons with EMEP and CASTNET observations for experiment XPT2 (without ammonia chemistry). Compare to Figure 3, statistics parameters are same as figure 2, but for XPT2.

Figure 8, Sulfate, nitrate and ammonium comparisons with EMEP and CASTNET observations for experiment XPT3 (without dust and sea salt). Compare to Figure 3, statistics parameters are same as figure 2, but for XPT3.

Figure 9, Differences of sulfate, nitrate and ammonium concentration between control run (CTL) and sensitivity 3 run (XPT3, without dust and sea salt aerosols).

Figure 10, Annual mean sulfate, nitrate and ammonium deposition fluxes distributions for CTL run.

Figure 11, Comparisons of depositions between model simulations and CASTNET-inferred measurements.

Acknowledgments:

This work was supported by NSF ATM-0321380 and OCE-0452972. We thank the two anonymous reviewers for their insightful comments.

References:

Avallone, L.M., and Prather, M.J., Tracer-tracer correlations: Three-dimensional model

simulations and comparison to observations, *J. Geophys. Res.*, 102, 19233-19246, 1997.

Balkanski, Y. J., Jacob, D. J., Gardner, G. M., Graustein, W. C., and Turekian, K. K., Transport and residence times of tropospheric aerosols inferred from a global three-dimensional simulation of ²¹⁰Pb aerosols, *J. Geophys. Res.*, 98, 20573-20586, 1993.

Bassett, M. E., and J. H. Seinfeld, Atmospheric equilibrium model of sulfate and nitrate aerosol, *Atmos. Environ.*, 17, 2237-2252, 1983.

Baughcum, S. I., T. G. Tritz, S. C. Henderson, and D. C. Pickett, Scheduled civil aircraft emission inventories for 1992: Database development and analysis, Tech. Rep. NASA CR-4700, Langley Res. Cent. Hampton, Va., 1996.

Bian, H., Improvement and application of UCI chemistry transport model, Ph.D thesis, 310 pp., Univ. of Calif., Irvine, Calif., 2001.

Bian, H., and M. J. Prather, Fast-J2: Accurate simulation of stratospheric photolysis in global chemistry models, *J. Atmos. Chem.*, 41, 281-296, 2002.

Bian, H., and C. S. Zender, Mineral dust and global tropospheric chemistry: Relative roles of photolysis and heterogeneous uptake, *J. Geophys. Res.*, 108, 4672, doi:10.1029/2002JD003143, 2003.

Chin, M., A.D.L. Savoie, B.J. Huebert, A.R. Bandy, D.C. Thomson, T.S. Bates, P.K. Quinn, E.S. Saltzman and W.J. De Bruyn, Atmospheric sulfur cycle simulated in the global model GOCART: Comparison with field observations and regional budgets, *J. Geophys. Res.*, 105, 24689-24712, 2000.

Clegg, S. L., P. Brimblecombe, and A. S. Wexler, A thermodynamic model of the

system H⁺-NH₄⁺-Na⁺-SO₄²⁻-NO₃⁻-Cl-H₂O at 298.15 K, *J. Phys. Chem.*, 102, 2155-2171, 1998a.

Clegg, S. L., P. Brimblecombe, and A. S. Wexler, A thermodynamic model of the system H⁺-NH₄⁺-Na⁺-SO₄²⁻-NO₃⁻-Cl-H₂O at tropospheric temperatures, *J. Phys. Chem.*, 102, 2137-2154, 1998b.

Charlson, R. J., J. E. Lovelock, M.O. Andreae, and S. G. Warren, Oceanic phytoplankton, atmospheric sulfur, cloud albedo and climate, *Nature*, 326, 655-661, 1987.

Coffman D.J., and D. Hegg, A preliminary study of the effect of ammonia on particle nucleation in the marine boundary layer, *J. Geophys. Res.*, 100, 7147-7160, 1995

Cohan, M.D., R.C. Flagan, and J.H. Seinfeld, Studies of concentrated electrolyte solutions using the electrodynamic balance, I. Water activities for mixed electrolyte solutions, *J. Phys. Chem.*, 91, 4563-4574, 1987a.

Cohan, M.D., R.C. Flagan, and J.H. Seinfeld, Studies of concentrated electrolyte solutions using the electrodynamic balance, I. Water activities for mixed electrolyte solutions, *J. Phys. Chem.*, 91, 4575-4582, 1987b.

Goodman, A. L., G. M. Underwood, and V.H. Grassian, A laboratory study of the heterogeneous reaction of nitric acid on calcium carbonate particles, *J. Geophys. Res.*, 105, 29053-29064, 2000.

EMEP report 2003, http://www.emep.int/common_publications.html/

Ginoux, P., M. Chin, I. Tegen, J. Prospero, B. Holben, O. Dubovik, and S.J. Lin, Sources and distributions of dust aerosols simulated with the GOCART model, *J.*

Geophys. Res., 106, 20273-20555, 2001.

Giorgi, F., and Chameides, W. L., Rainout lifetimes of highly soluble aerosols and gases as inferred from simulation with a general circulation model. *J. Geophys. Res.*, 91, 14367-14376, 1986.

Heintzenberg, J., Fine particles in the global troposphere: A review, *Tellus*, Ser. B., 41, 149-160, 1998.

Hall, T.M., and Prather, M.J., Simulations of the trend and annual cycle in stratospheric CO₂, *J. Geophys. Res.*, 98, 10573-10581, 1993.

Hsu, Juno, M. J. Prather, O. Wild, J.K. Sundet, I.S.A. Isaksen, E.V. Browell, M.A. Avery, G.W. Sachse, Are the TRACE-P measurements representative of the Western Pacific during March 2001, *J. Geophys. Res.*, 109(D02 314), doi:10.1029/2003JD004002, 2004.

Hannegan, B.J., Olsen, S.C., Prather, M.J., Zhu, X., Rind, D., and Lerner, J., The dry stratosphere: a limit on cometary influx, *Geophys. Res. Lett.*, 25, 1649-1652, 1998.

Jacob, D.J., Prather, M.J., et al., Evaluation and intercomparison of global atmospheric transport models using ²²²Rn and other short-lived tracers, *J. Geophys. Res.*, 102, 5953-5970, 1997.

Kim, Y. P., J. H. Seinfeld, and P. Saxena, Atmospheric gas/aerosol equilibrium, I. Thermodynamic model, *Aerosol Sci. Technol.*, 19, 157-181, 1993a.

Kim, Y. P., J. H. Seinfeld, and P. Saxena, Atmospheric gas/aerosol equilibrium, II. Analysis of common approximations and activity coefficient calculation methods, *Aerosol Sci. Technol.*, 19, 182-198, 1993b.

Kim, Y. P., J. H. Seinfeld, and P. Saxena, Atmospheric gas/aerosol equilibrium, III, Thermodynamics of crustal elements Ca²⁺, K⁺, and Mg²⁺, *Aerosol Sci. Technol.* 22, 93-110,1995.

Lauer, A, J. Hendricks, I. Ackermann, B. Schell, H. Hass, and S. Metzger, Simulating aerosol microphysics with the ECHAM/MADE GCM Part I: Model description and comparison with observations, *ACPD*, 2005.

Luo, C., N.M. Mahowald, J. del Corral, Sensitivity study of meteorological parameters on mineral aerosol mobilization, transport, and distribution, *J. Geophys. Res.*, 108, 4447, doi:10.1029/2003JD003483, 2003.

Mahowald, N.M., C. Luo, J. del Corral, and C.S. Zender, Interannual variability in atmospheric mineral aerosols from 22-year model simulation and observational data, *J. Geophys. Res.*, 108, 4352, doi:10.1029/2002JD002821, 2003.

McLinden, C.A., Olsen, S.C., Hannegan, B., Wild, O., Prather, M.J., and Sundet, J., Stratospheric ozone in 3-D models: A simple chemistry and the cross-tropopause flux, *J. Geophys. Res.*, 105, 14653-14665, 2000.

McLinden, C. A., M. J. Prather, and M. S. Johnson, Global modeling of the isotopic analogues of N₂O: Stratospheric distributions, budgets, and the 17O – 18O mass-independent anomaly, *J. Geophys. Res.*, 108(D8), 4233, doi:10.1029/2002JD002560, 2003.

Meng, Z., and J. H. Seinfeld, Time scales to achieve atmospheric gas/aerosol equilibrium for volatile species, *Atmos. Environ.*, 30, 2889-2900, 1996.

Metzger, S. M., Gas/Aerosol Partitioning: A simplified Method for

Global Modeling, Ph.D. Thesis, University Utrecht, The Netherlands,
ISBN:90-393-2510-3,

<http://www.library.uu.nl/digiarchief/dip/diss/1930853/inhoud.htm>, pdf
file, 2000.

Metzger, S., F. Dentener, S. Pandis, and J. Lelieveld, Gas/aerosol partitioning: I. A
computationally efficient model, *J. Geophys. Res.*, 107, 4312, 10.1029/2001JD001102,
2002a.

Metzger, S., F. Dentener, M. Krol, A. Jeuken, and Lelieveld, Gas/aerosol partitioning,
2. Global modeling results, *J. Geophys. Res.*, 107, 4313, 10.1029/2001JD001103,
2002b.

Metzger, S. M., N. Mihalopoulos, J. Lelieveld, Importance of mineral
cations and organics in gas-aerosol partitioning of reactive nitrogen
compounds: case study based on MINOS results, *Atmos. Chem.
Phys.*, vol,6, 2549-2567, 2006.

Michel, A. E., C. R. Usher, and V. H. Grassian, Heterogeneous and
catalytic uptake of ozone on mineral oxides and dusts: A Knudsen
cell investigation, *Geophys. Res. Lett.*, 29(14), 1665,
doi:10.1029/2002GL014896, 2002.

Monahan, E., D. Spiel, and K. Spiel, 1986: *Oceanic Whitecaps*. Reidel.

Nenes, A., C. Pilinis, and S.N. Pandis, Isorropia: A new thermodynamic model for
multiphase multicomponent inorganic aerosols, *Aquat. Geochem.*, 4, 123-152, 1998.

National Research Council (NRC) (1996), *Aerosol Radiative Forcing and Climate
Change*, Natl. Acad. Press, Washington, D.C.

Olsen, S.C., Hannegan, B.J., Zhu, X., and Prather, M.J., Evaluating ozone depletion from very short-lived halocarbons, *Geophys. Res. Lett.*, 27, 1475-1478, 2000.

Prather, M.J., MeElroy, M.B., Wofsy, S.C., Russell, G., and Rind, D., Chemistry of the global troposphere: Fluorocarbon as tracers of air motion, *J. Geophys. Res.*, 92, 6579-6613, 1987.

Prather, M.J., and D. Ehhalt, Atmospheric chemistry and greenhouse gases, in *Climate Change 2001, the Scientific Basis*, edited by J. E. A. Houghton, pp. 239-288, Cambridge Univ. press, New York, 2001.

Price, C., and D. Rind, A simple lightning parameterization for calculating global lightning distributions, *J. Geophys. Res.*, 97, 9919-9933, 1992.

Smith, M. H., P. M. Park, and I. E. Consterdine, 1993: Marine aerosol concentration and estimated fluxes over sea. *Quart. J. Roy. Meteor. Soc.*, **119**, 809–824.

Stockes, R.H., and R. A. Robinson, Interactions in aqueous nonelectrolyte solutions, I. Solute solvent equilibria, *J. Phys. Chem.*, 70, 2126-2130, 1966.

Tsigaridis, K., M. Krol, F. J. Dentener, Y. Balkanski, J. Lathire, S. Metzger, D. A. Hauglustaine and M. Kanakidou, Change in global aerosol composition since preindustrial times, *ACPD*, <http://www.copernicus.org/EGU/acp/acpd/>, 2006.

Underwood, G. M., C. H. Song, M. Phadnis, G. R. Carmichael and V. H. Grassian, Heterogeneous reactions of NO₂ and HNO₃ on oxides and mineral dust: A combined laboratory and modeling study, *J. Geophys. Res.*, 106, 22931-22964, 2001.

Wang, Y., D.J. Jacob, and J.A. Logan, Global simulation of tropospheric O₃-NO_x-

Hydrocarbon chemistry: 2. Model formation, *J. Geophys. Res.*, 103, 10713-10725, 1998a.

Wesely, M. L., and B. B. Hicks, Some factors that affect the deposition rates of sulfur dioxide and similar gases on vegetation, *J. Air Pollut. Control Assoc.*, 27, 1110-1116, 1977.

Wexler, A. S., and J. H. Seinfeld, Second-generation inorganic aerosol model, *Atmos. Environ.*, part A, 25, 2731-2748, 1991.

Wild, O., and M. J. Prather, Excitation of the primary tropospheric chemical mode in a global three-dimensional model, *J. Geophys. Res.*, 105, 24647-24660, 2000.

Wild, O., and Akimoto, Intercontinental transport of ozone and its precursors in a three-dimensional global CTM, *J. Geophys. Res.*, 106, 27729-27744, 2001.

Zdanovskii, A.B., New methods of calculating solubilities of electrolytes in multicomponent systems, *Zh. Fiz. Khim.*, 22, 1475-1485, 1948.

Wild, O., J. K. Sundet, M. J. Prather, I. S. A. Isaksen, H. Akimoto, E. V. Browell, and S. J. Oltmans (2003), *J. Geophys. Res.*, 108, 8826, doi:10.1029/2002JD003283.

Wild, Oliver, M. J. Prather, H. Akimoto, J. K. Sundet, I. S. A. Isaksen, J. H. Crawford, D. D. Davis, M. A. Avery, Y. Kondo, G. W. Sachse, S. T. Sandholm, CTM Ozone Simulations for Spring 2001 over the Western Pacific: Regional ozone production and its global impacts, *J. Geophys. Res.*, 109(D15), D15S02, doi:10.1029/2003JD004041, 2004.

Zender, C. S., H. Bian, and D. Newman, Mineral Dust Entrainment and Deposition (DEAD) model: Description and 1990s dust climatology, *J. Geophys. Res.*, 108, 4416,

doi:10.1029/2002JD002775, 2003.

Zhang, Y., and G. R. Carmichael, The role of mineral aerosol in tropospheric chemistry in East Asia: A model study, *J. Appl. Meteorol.*, 38, 353-366, 1999.

Table 1, Correlations of aerosols between observation and model simulation

	SO4~NH4	NO3~NH4	SO4~NO3
OBS.	0.81	0.71	0.52
MDL.	0.93	0.57	0.49

Table 2, Correlations and regression parameters between observations and simulations for different runs

	CTL			XPT1			XPT2			XPT3		
	r	m	b	r	m	b	r	m	b	r	m	B
SO4 (CASTNET)	.81	.56	.43	.75	.41	.47	.82	.12	.07	.50	.24	.49
NO3 (CASTNET)	.41	.22	.18	.31	.18	.21	-.14	-.017	.027	.50	.55	.26
NH4 (CASTNET)	.74	.61	.45	.64	.46	.51	-	-	-	.75	.55	.56
SO4 (EMEP)	.45	.32	.98	.23	.21	1.27	-.2	-.02	.39	.51	.21	.59
NO3 (EMEP)	.67	.44	.19	.69	.48	.22	.54	.043	.016	.50	.41	.52
NH4 (EMEP)	.46	0.34	.97	.47	.35	1.09	-	-	-	.50	.33	1.03

*Linear correlation coefficient r, and best fit parameters to $y=mx+b$ where x are observed data and y are simulated.

Table 3, Model (RMS_{abs}), (RMS_{rel}) and mean relative biases (MRB)
for different sensitivity runs

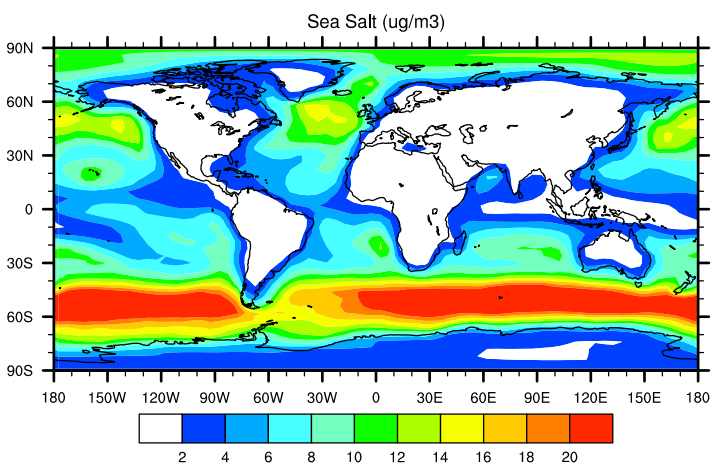
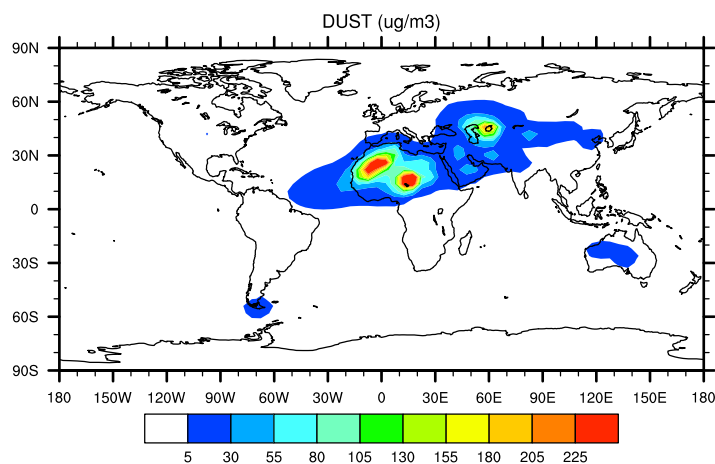
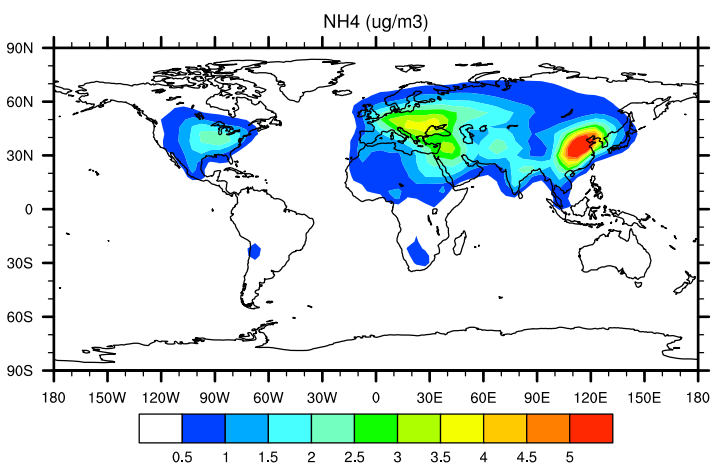
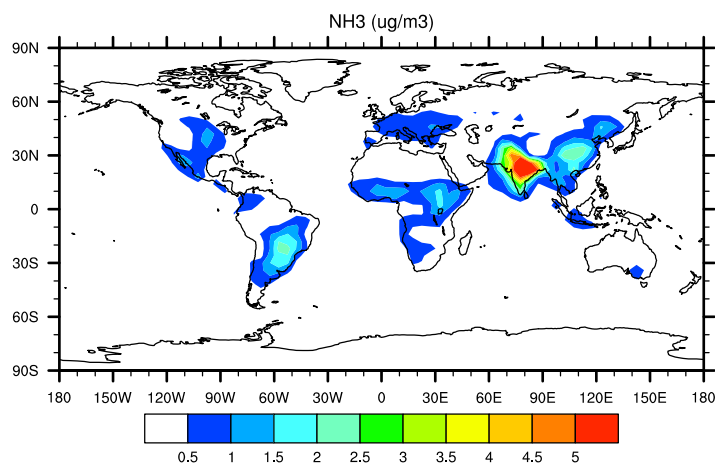
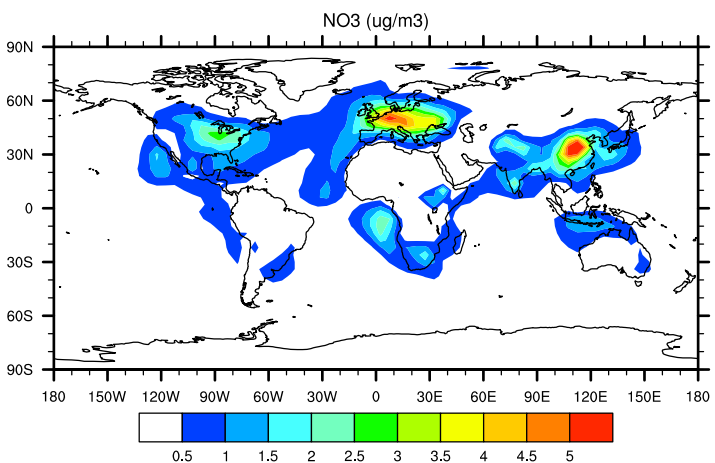
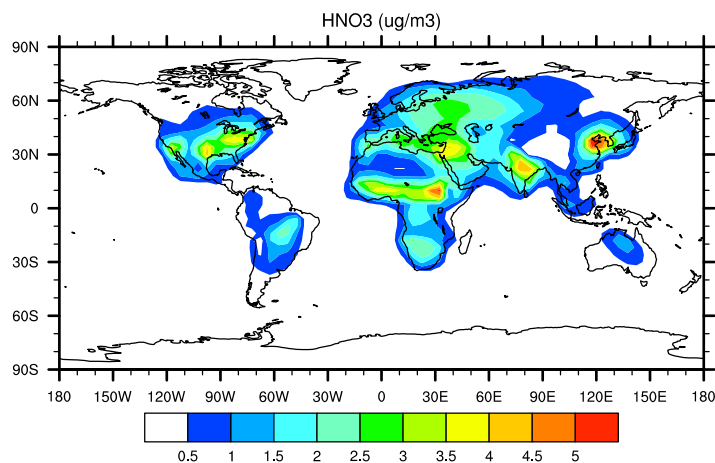
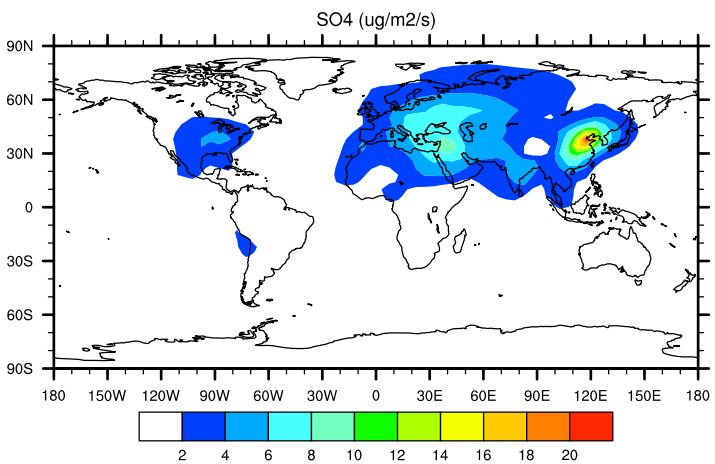
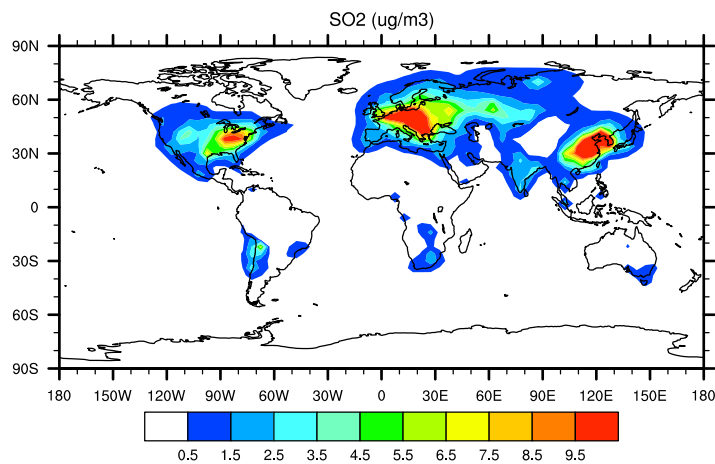
	CTL	XPT1	XPT2	XPT3
SO4 (RMS_{abs})	0.59	0.76	1.16	0.72
NO3 (RMS_{abs})	0.25	0.26	0.46	0.35
NH4 (RMS_{abs})	0.64	0.68	-	0.62
SO4 (RMS_{rel})	0.62	1.22	0.76	0.87
NO3 (RMS_{rel})	1.57	1.95	0.82	2.80
NH4 (RMS_{rel})	1.54	1.66	-	1.82
SO4 (MRB)	-0.33	-0.39	0.65	-0.65
NO3 (MRB)	-0.70	-0.96	0.79	-1.75
NH4 (MRB)	-0.66	-0.70	-	-0.83

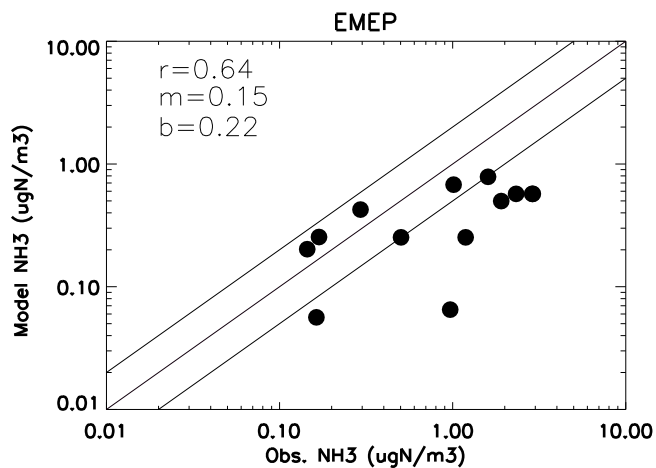
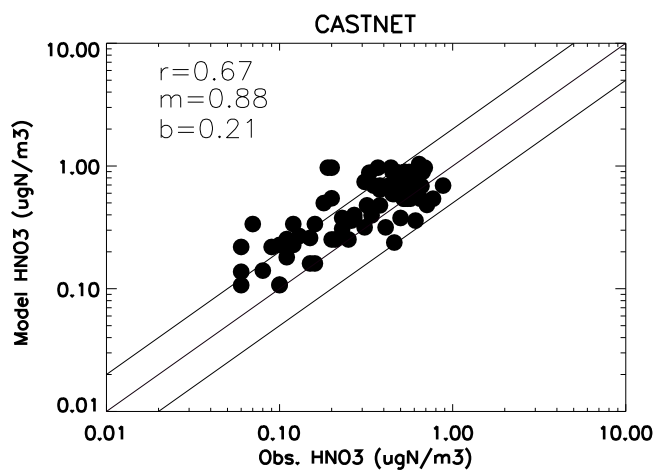
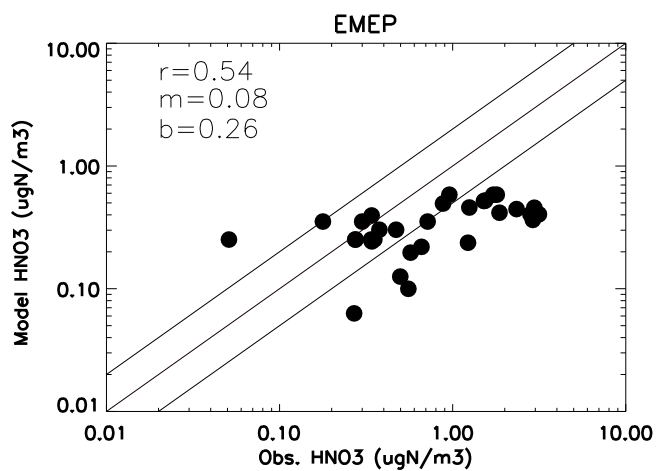
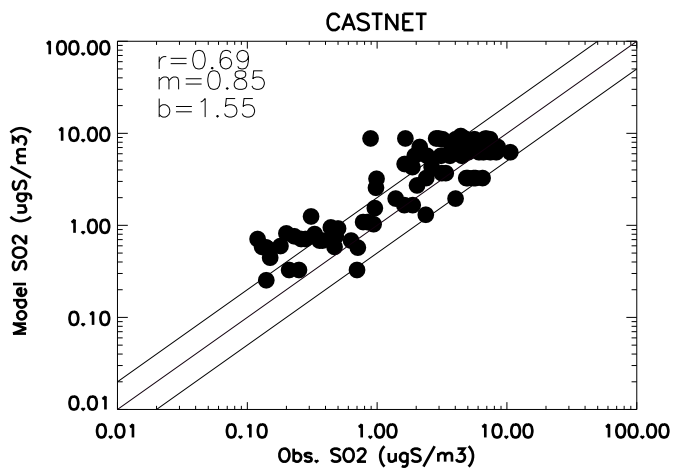
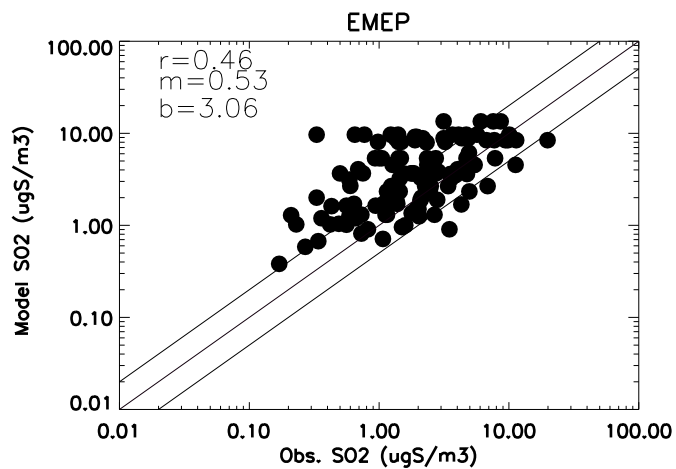
Table 4, Deposition fluxes comparison (Tg/yr)*

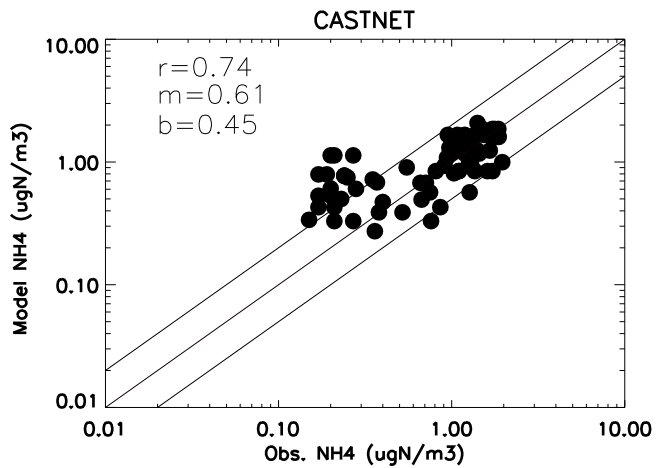
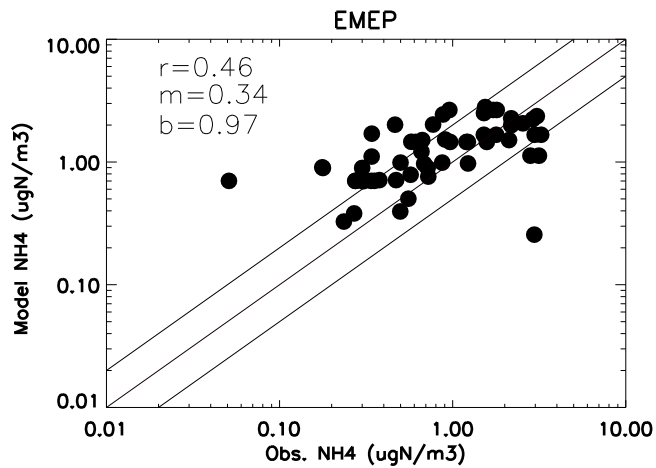
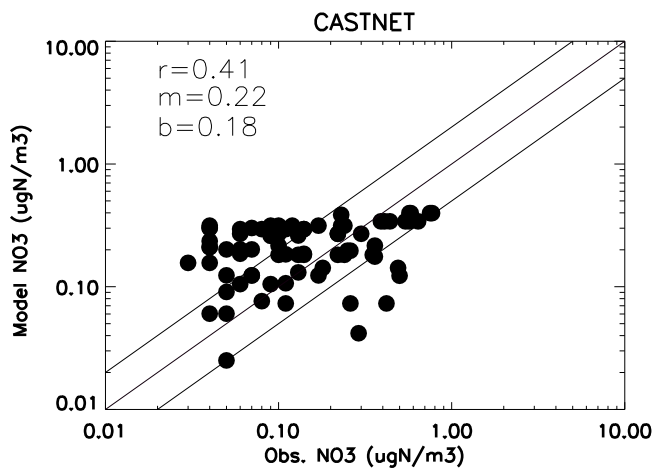
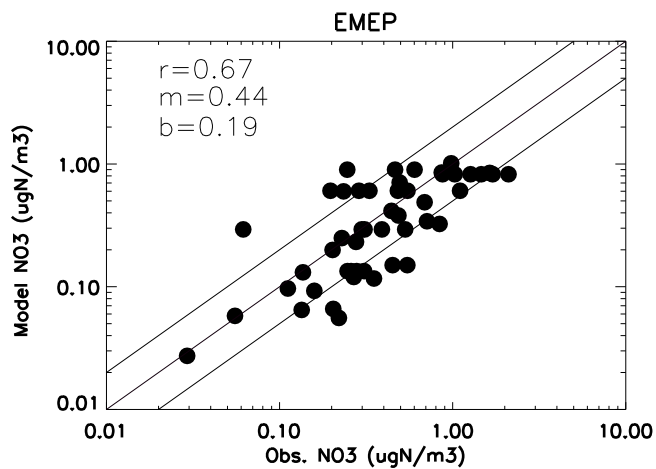
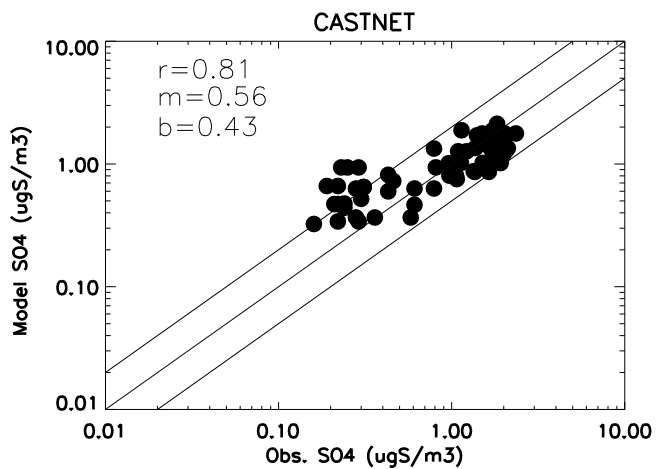
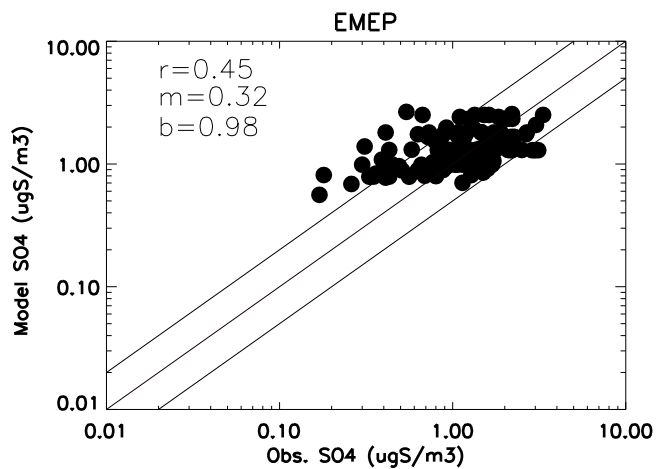
	Adam (1999)	Chin et al. (2002)	Dentener et al., (1994)	Duce et al., (1991)	Rodriguez et al.,(2004)	This work (present)	This work (pre- industrial)	This work (IPCC B1)*	This work (IPCC A1B)*
NH4	26.1	-	24.8	13.3	27	24.8	11.55	15.34	18.38
NO3	-	-	-	11.4	-	14.8	7.38	18.99	24.94
SO4	-	39.8	-	-	37.96	32.7	7.14	16.69	17.51
NH3	-	-	-	-	-	33.3	33.3	38.2	41.7
HNO3	-	-	-	-	-	39.9	14.9	39.7	26.0

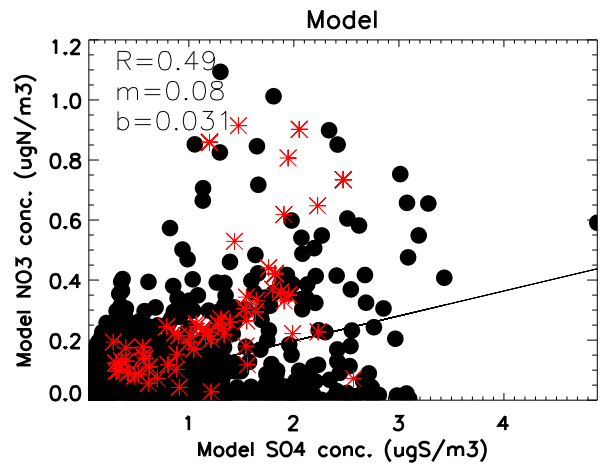
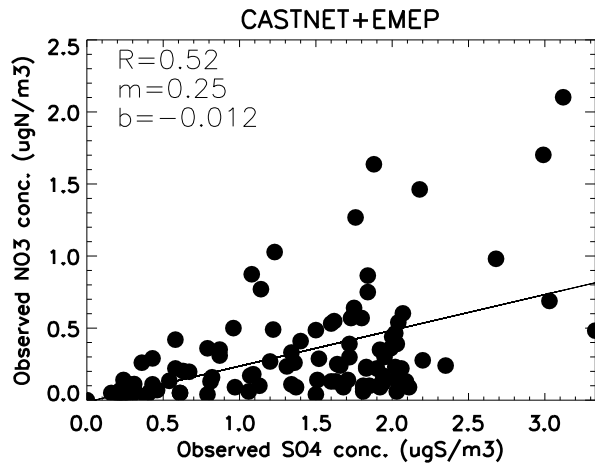
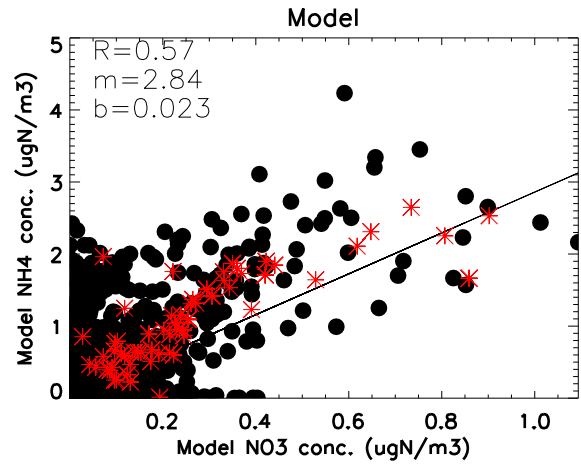
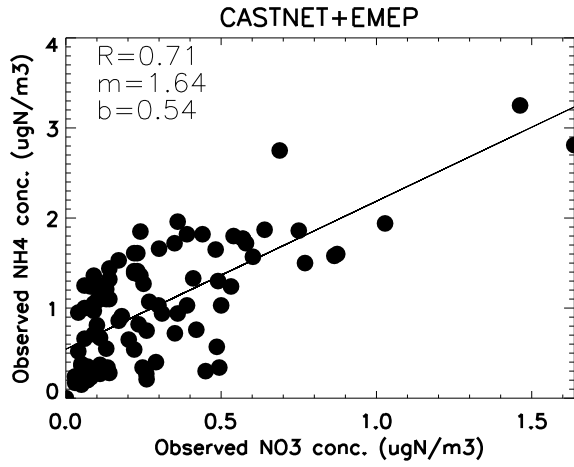
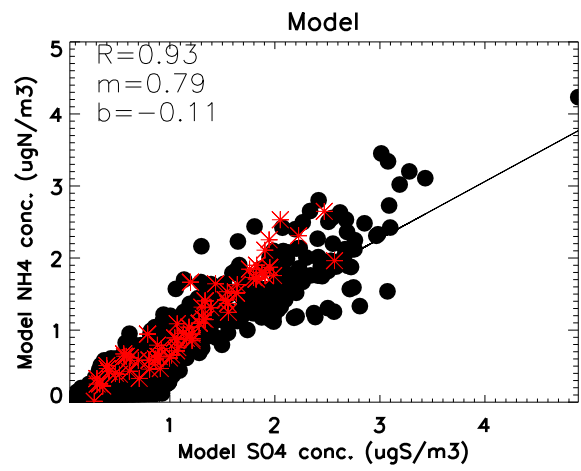
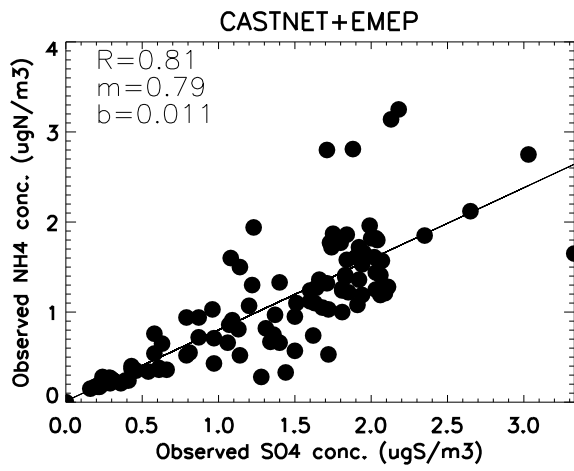
*: NH4, NO3, NH3 and HNO3 depositions as Tg N/yr; and SO4 deposition as Tg S/yr.

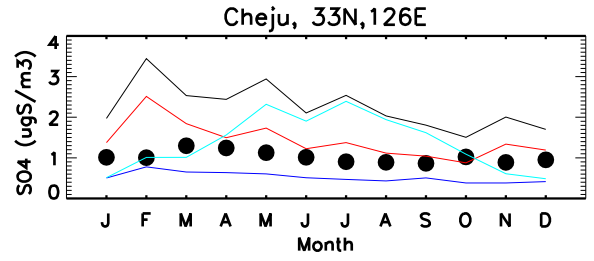
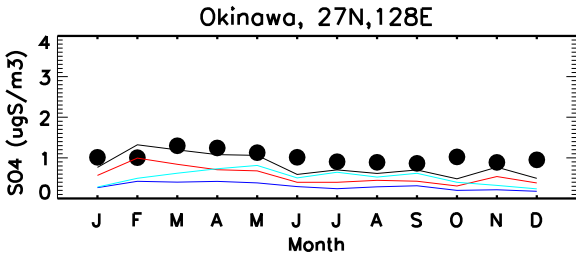
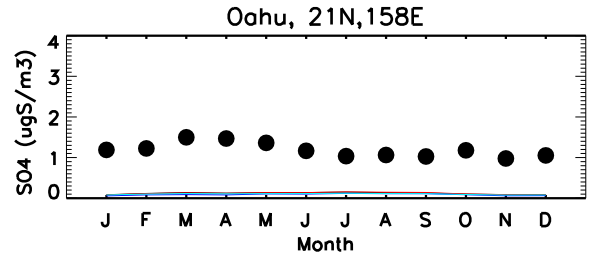
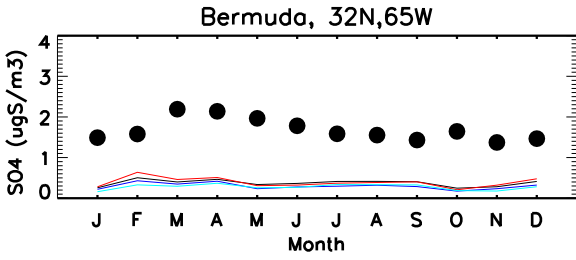
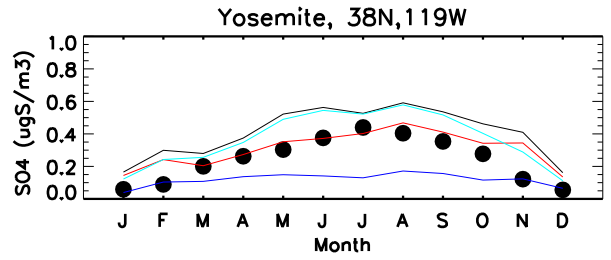
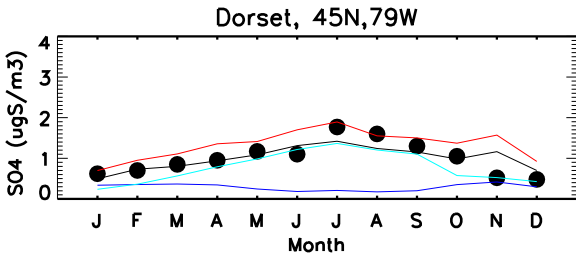
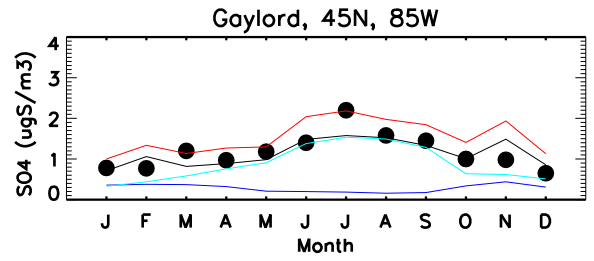
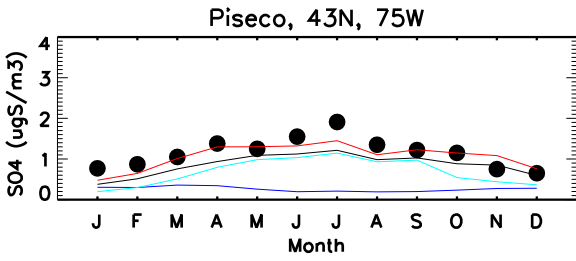
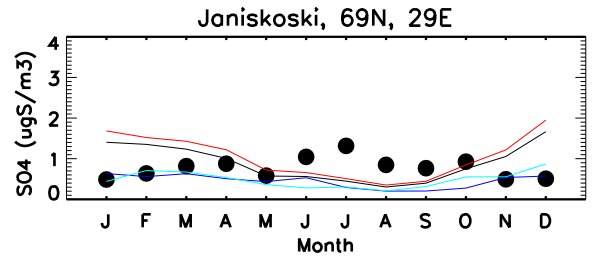
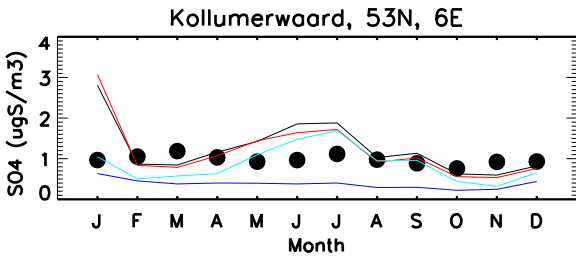
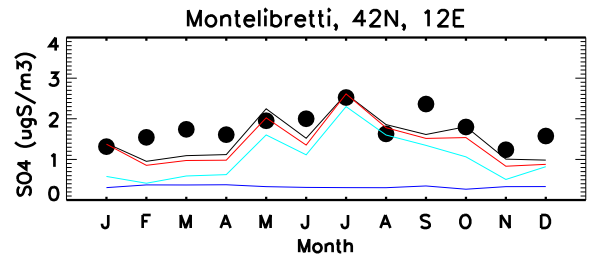
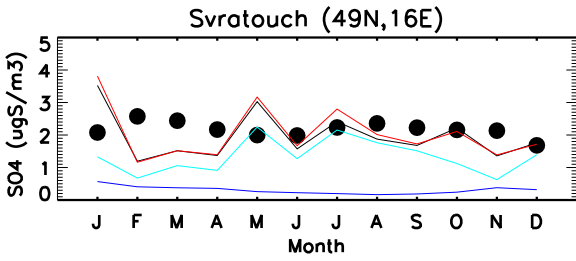
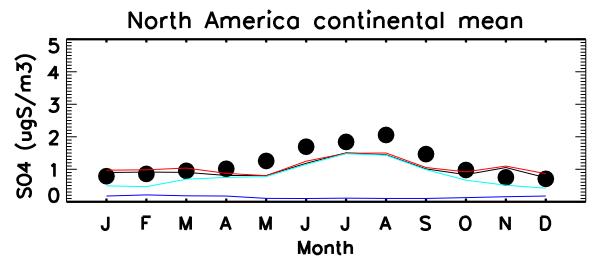
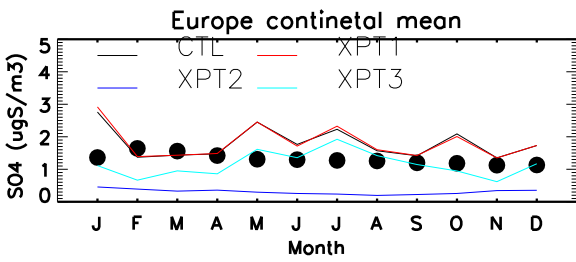
- *: IPCC B1 2010 scenario.
- *: IPCC A1B 2010 scenario.

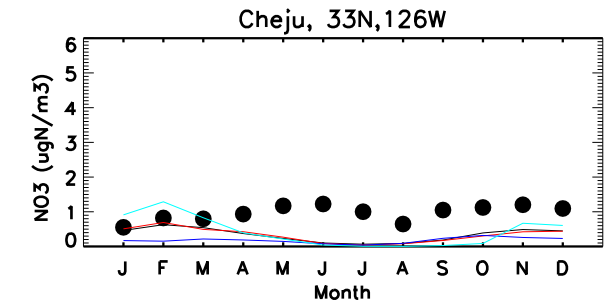
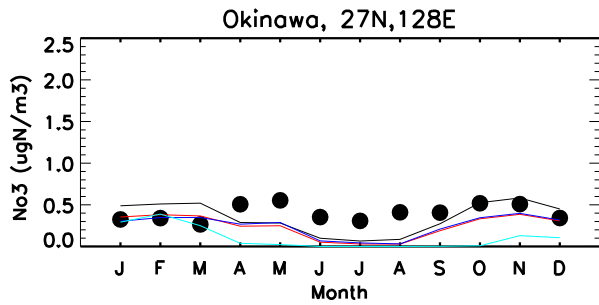
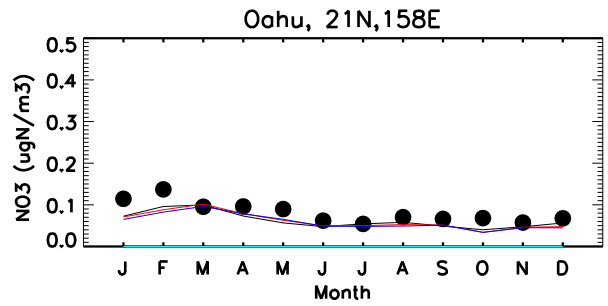
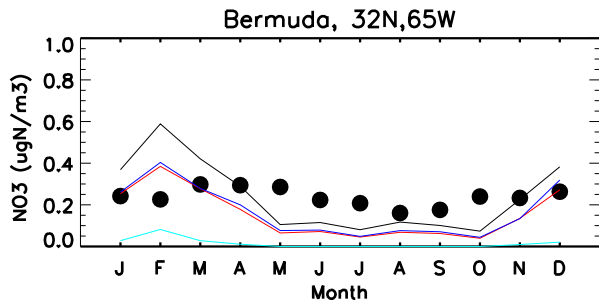
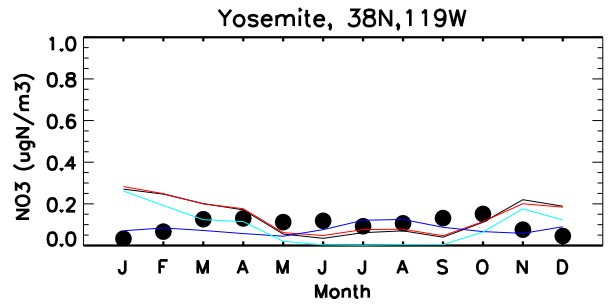
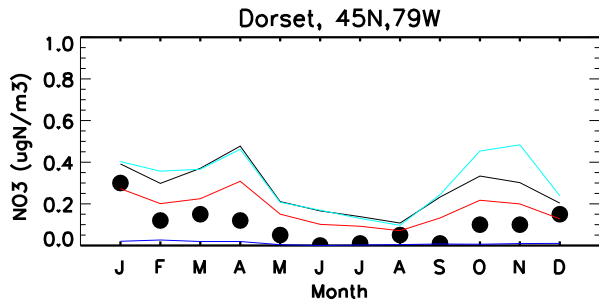
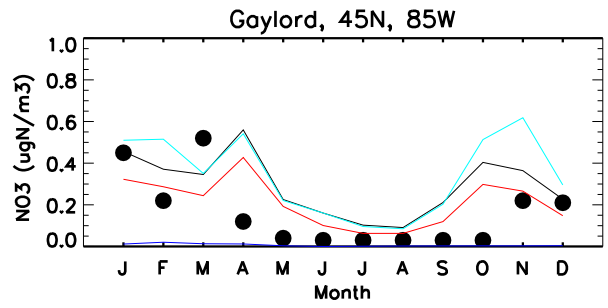
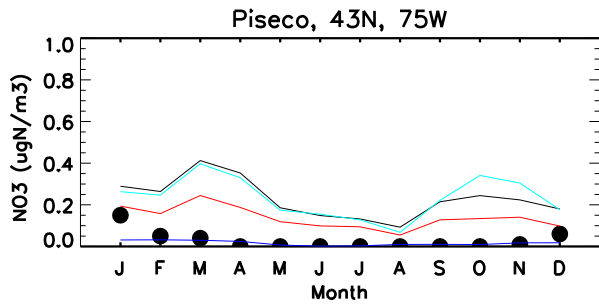
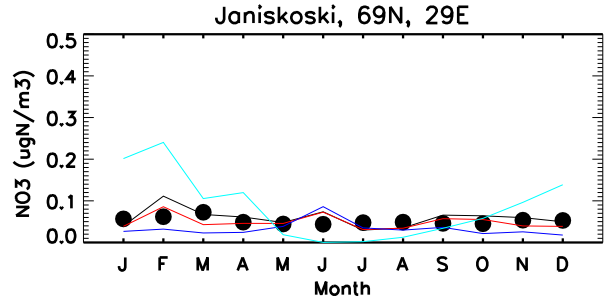
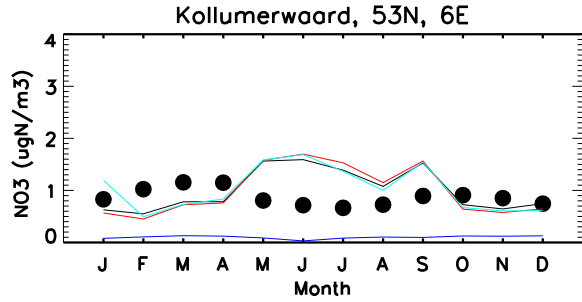
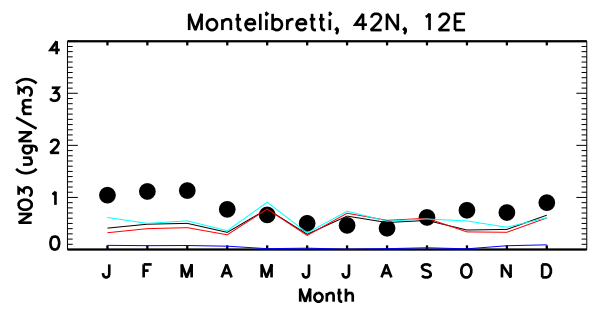
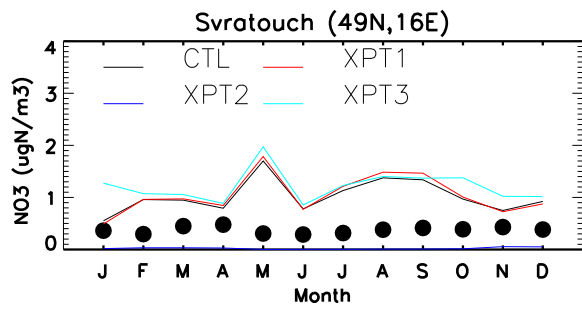


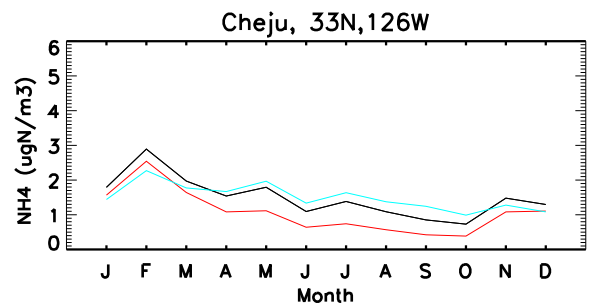
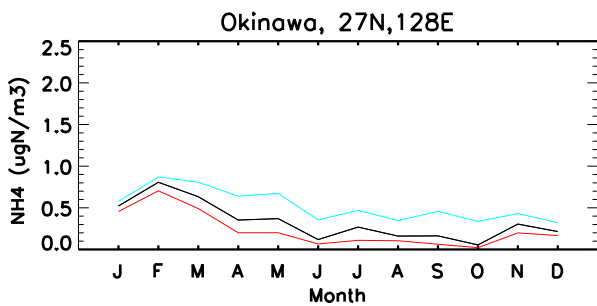
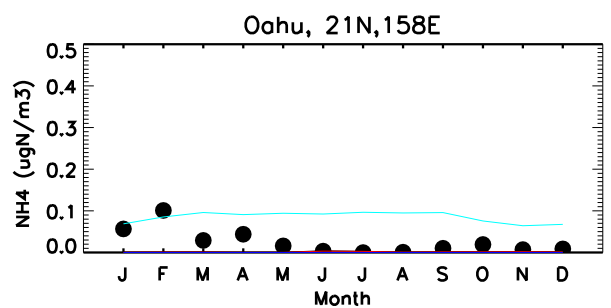
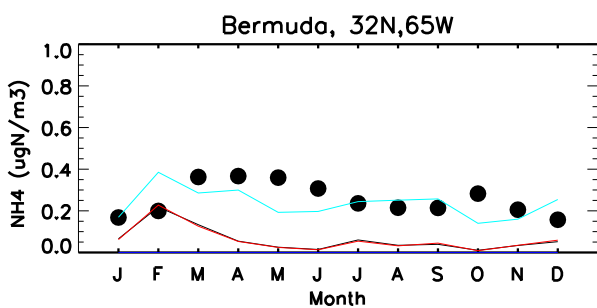
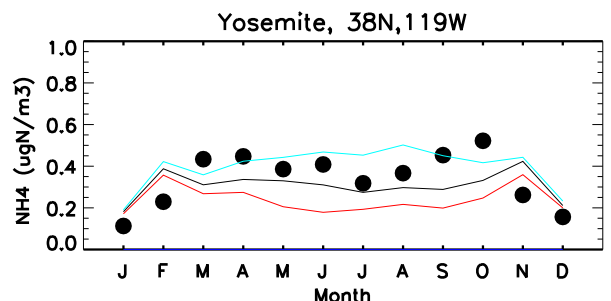
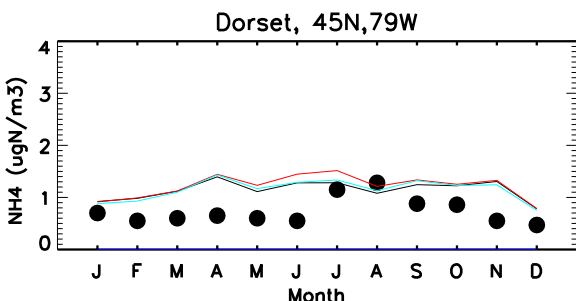
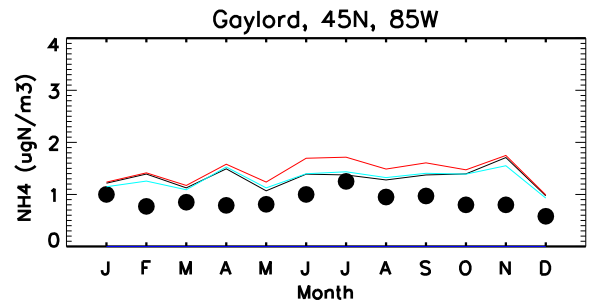
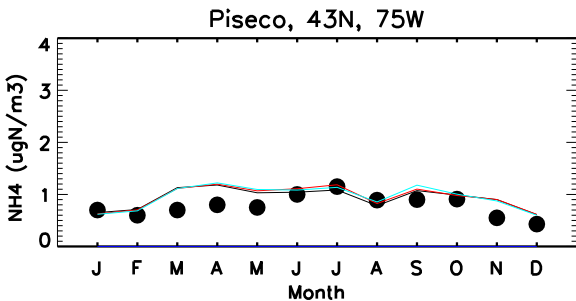
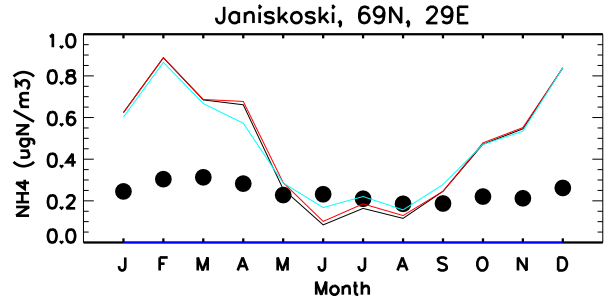
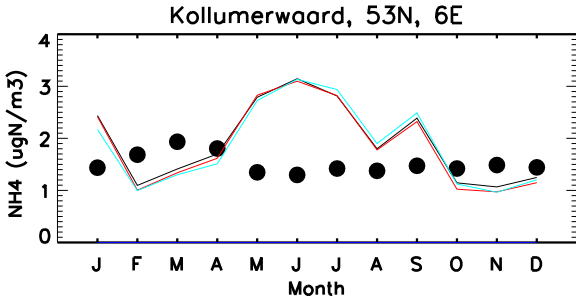
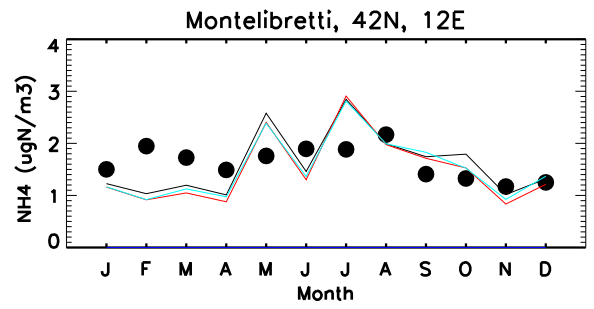
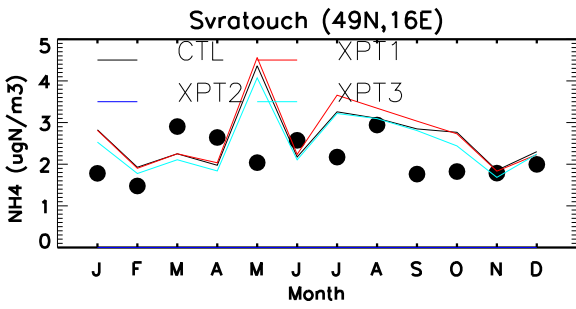


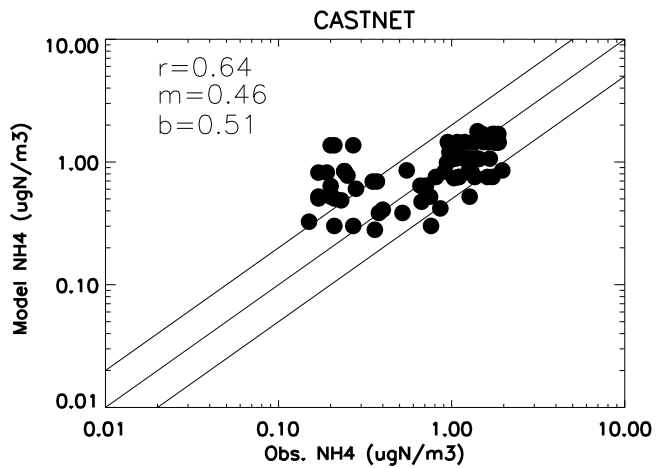
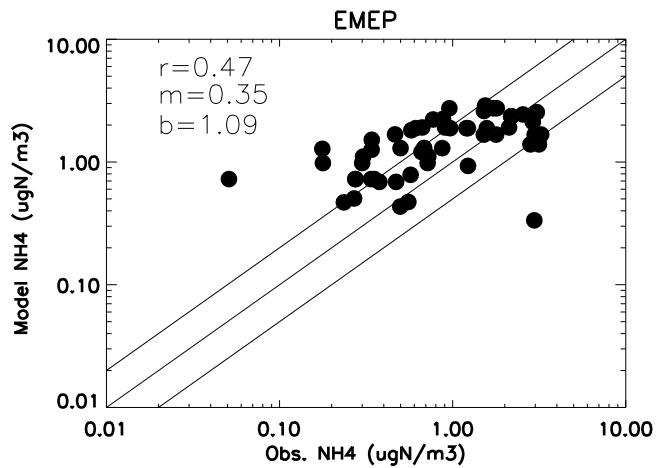
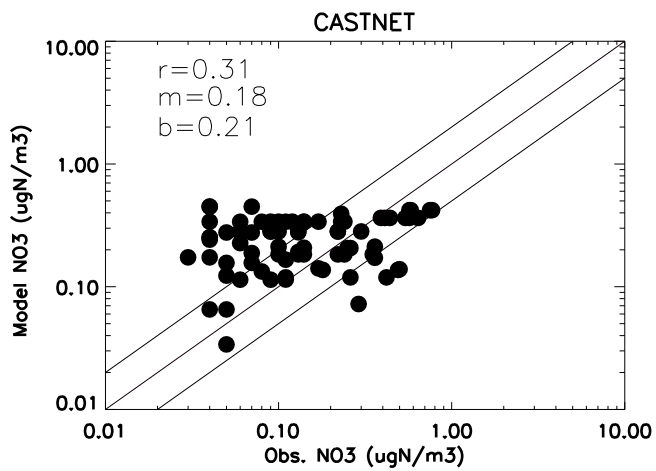
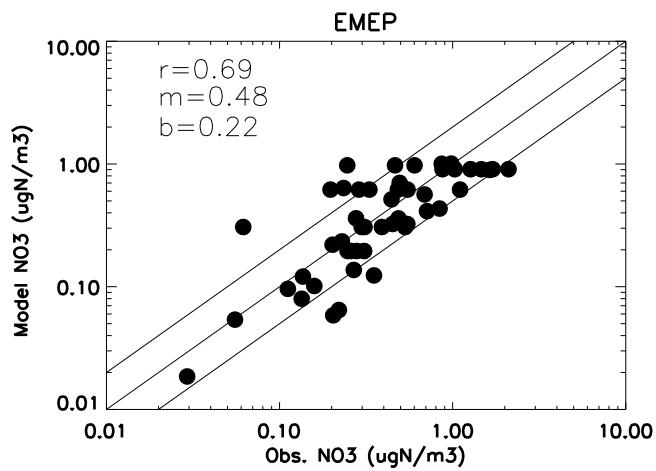
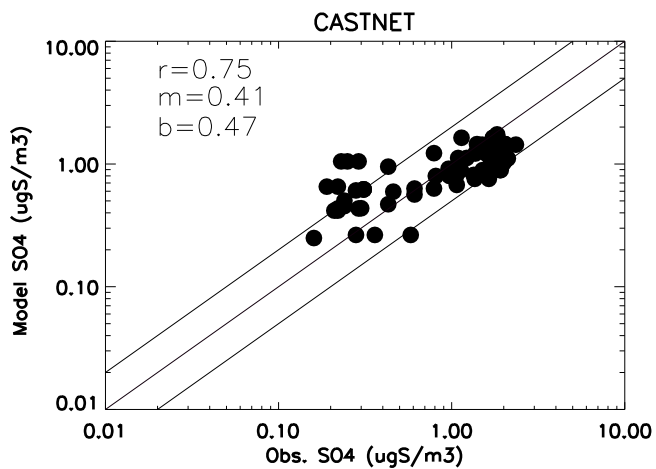
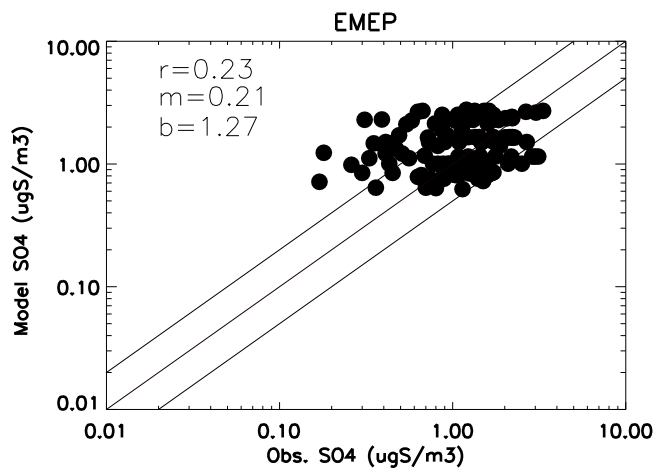


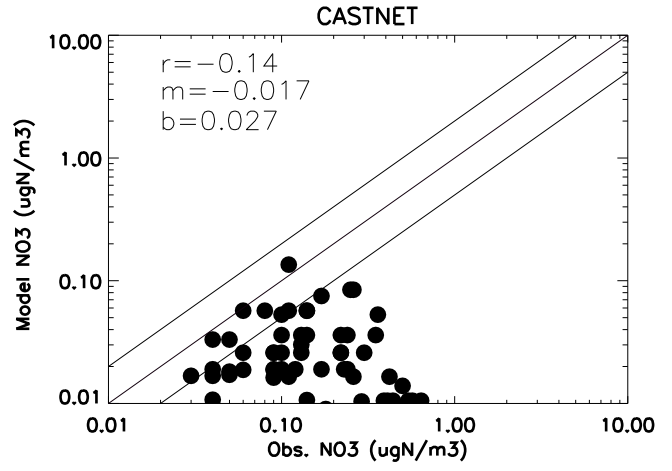
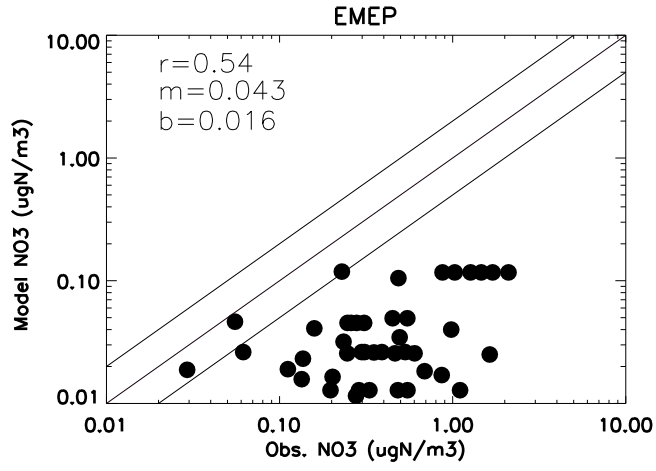
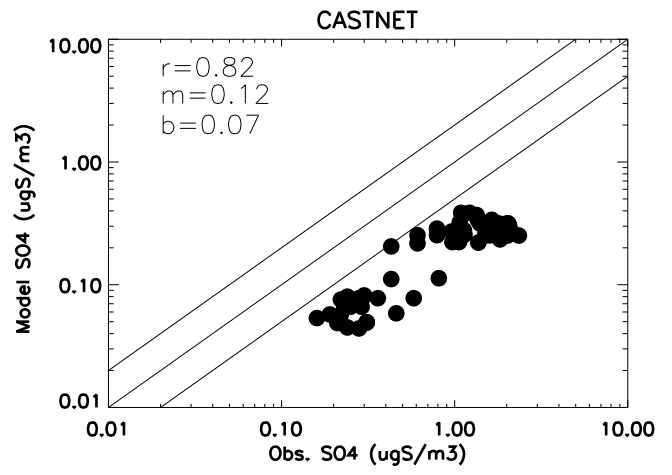
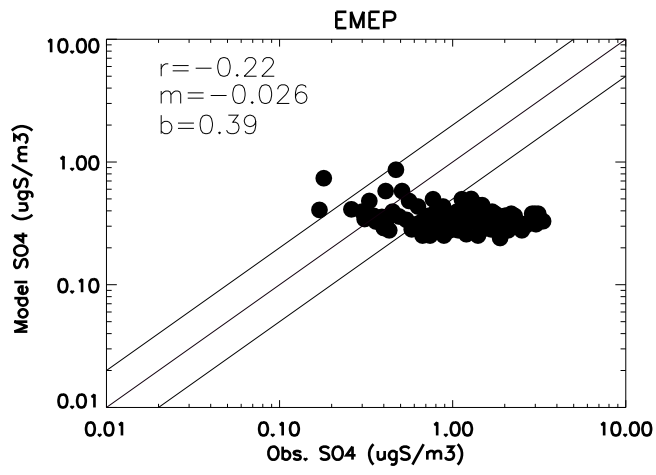


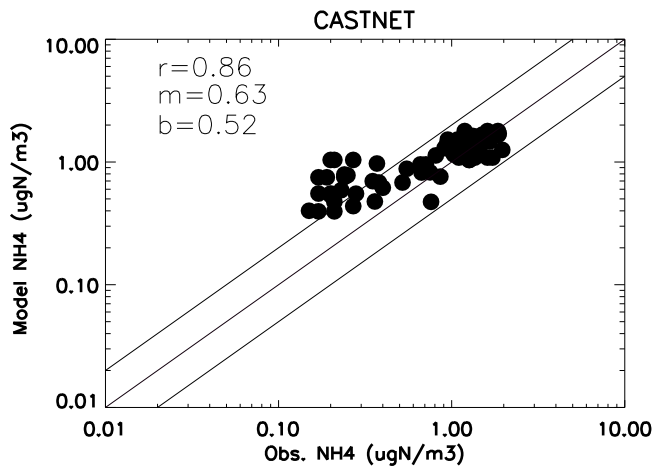
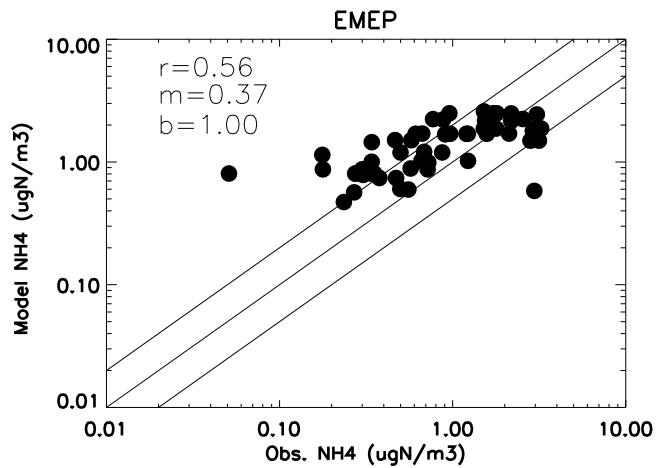
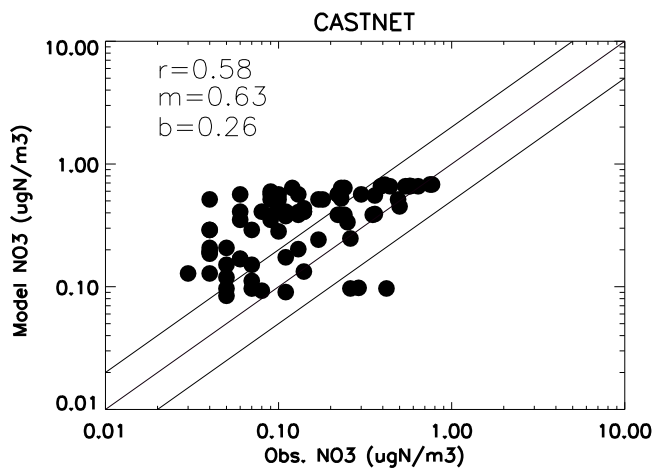
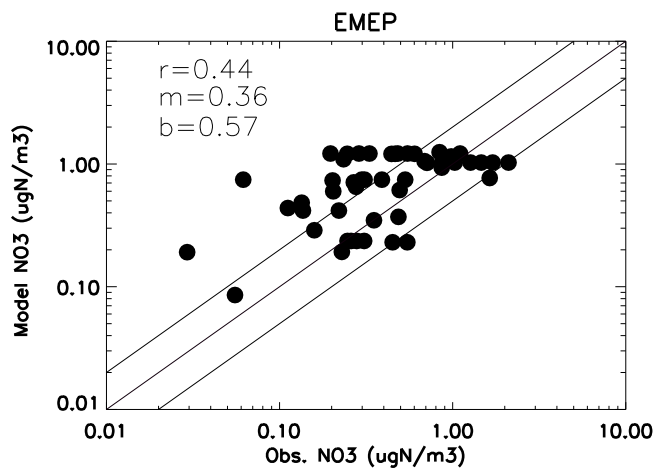
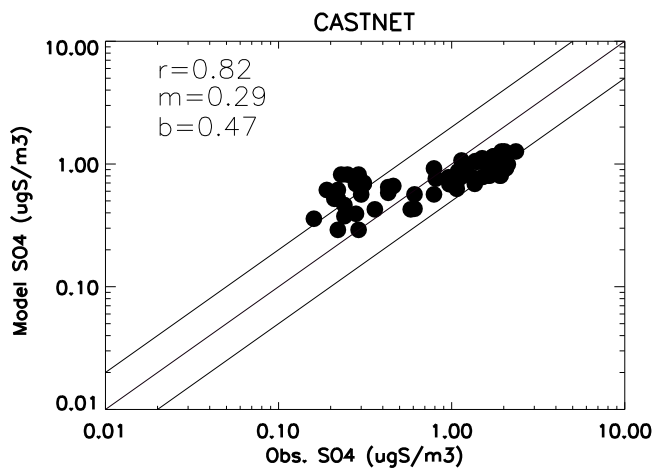
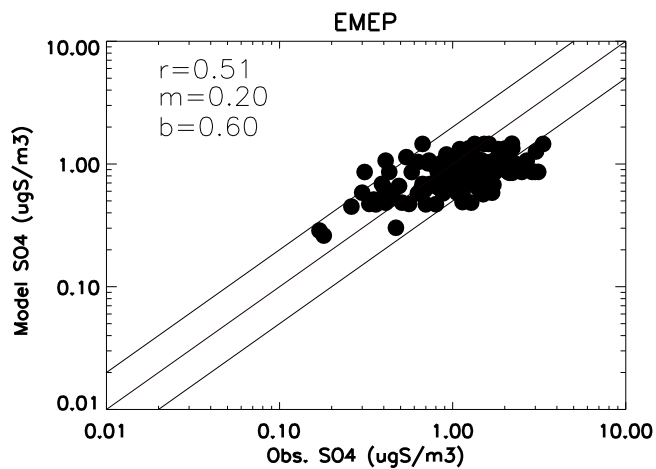




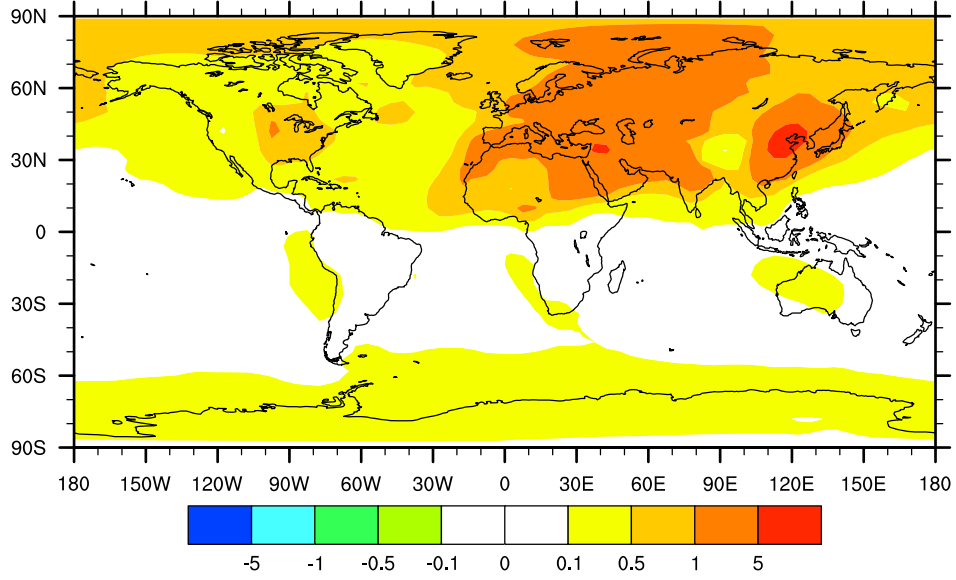




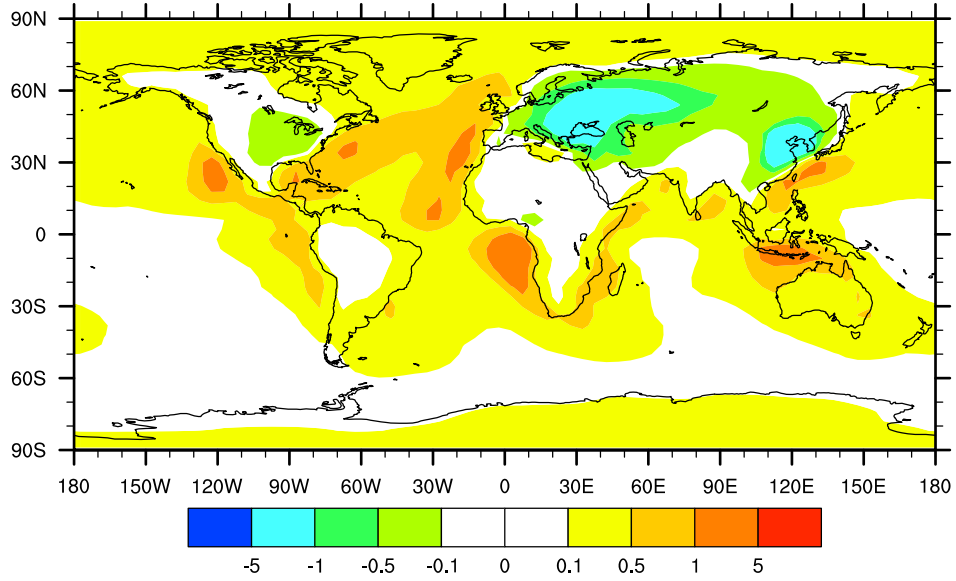




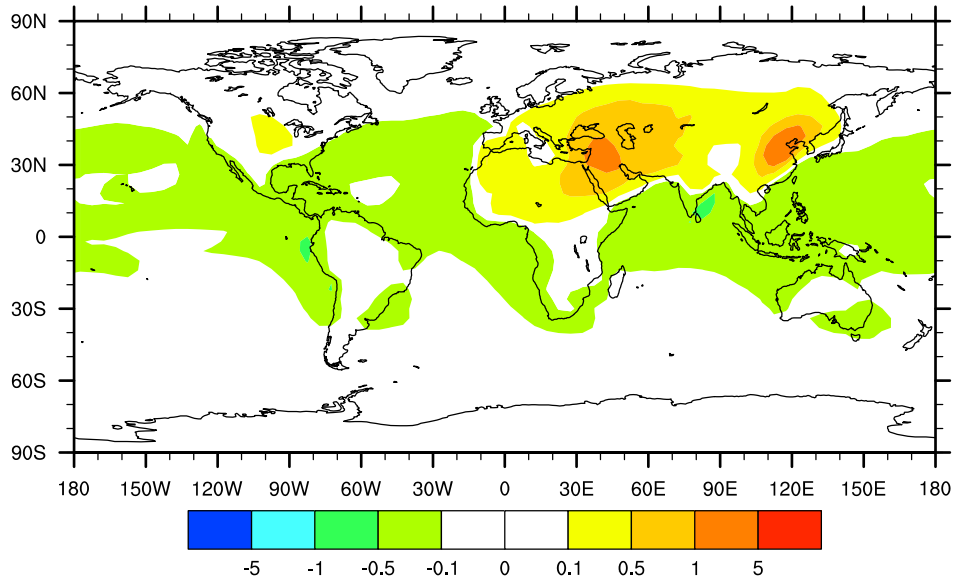
SO4 diff. of CTL-XPT3 (ug/m3)



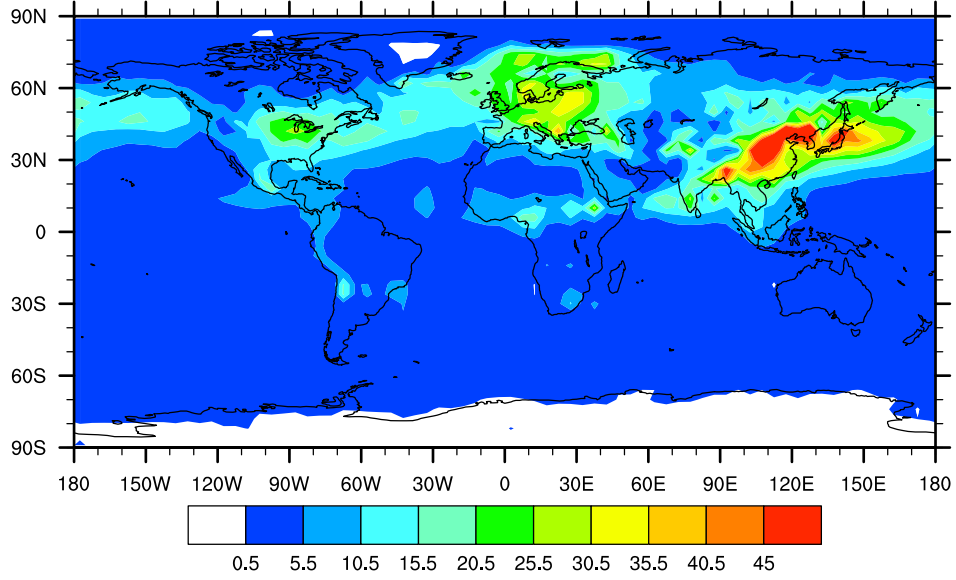
NO3 diff. of CTL-XPT3 (ug/m3)



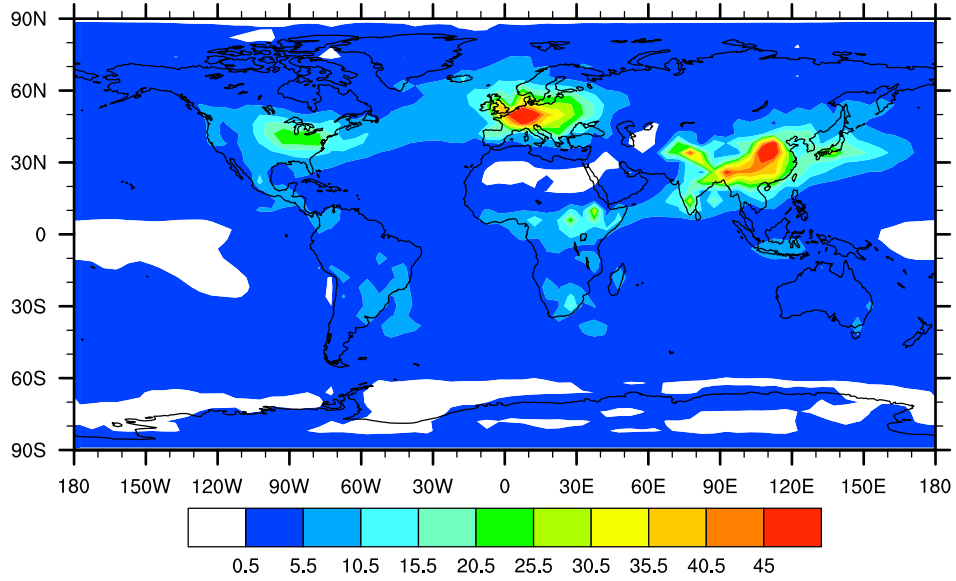
NH4 diff. of CTL-XPT3 (ug/m3)



SO4 dep. (ug/m2/s)



NO3 dep. (ug/m2/s)



NH4 dep. (ug/m2/s)

